IJCE

Printed by
Diagnosis Engineering & Technology Corp., Japan

International Journal of Comprehensive Engineering

ISSN 2186-2680
Volume 3, Number 1, March 2014

IJCE

Published by
International Association of Comprehensive Engineering (IACE)

http://www.iace-journal.org/

Honorary Editors

Toshio TOYOTA , Japan Institute of Condition Diagnosis Technology, Japan

Jinji GAO, Academician of the Chinese Academy of Engineering (CAE)

Hisayoshi MATSUYAMA, Vice-president The Society of Plant Engineers Japan

Editor-In-Chief

Peng CHEN
Mie University, 1577 Kurimamachiya-cho,Tsu-shi, Mie-ken, 514-8507 Japan
E-mail : chen@bio.mie-u.ac.jp

Associate Editors

Zhengjia HE, Xi'an Jiaotong University, China
E-mail: hzj@mail.xjtu.edu.cn

Maria Q. FENG, University of California, USA
E-mail: mfeng@uci.edu

Tadao KAWAI, Osaka City University, Japan
E-mail: kawai@mech.eng.osaka-cu.ac.jp

Susumu OKUMURA, University of Shiga Prefecture, Japan
E-mail: okumura.s@usp.ac.jp

Lei Li, Faculty of Science and Engineering Hosei University, Japan
E-mail:lilei@k.hosei.ac.jp

Huaqing WANG, Beijing University of Chemical Technology, China
E-mail: hqwang@mail.buct.edu.cn

Editorial Board

Changzheng CHEN, Shenyang University of Technology, China

Jin CHEN, Shanghai Jiaotong University, China

Fulei CHU, Tsinghua University, China

Zhiqian DONG, China development investment company

Lixin GAO, Beijing University of Technology, China

Jie HAN, Zhengzhou University, China

Min HU, Agent Director, China Plant Engineering Editorial office

Niaoqing HU, National University of Defense Technology, China

Jianping HU, Jiangsu University, China

Lixin LU, Jiangnan University, China

Ke LI, Jiangnan University, China

Hanping MAO, Jiangsu University, China

Zhongxing Li, Jiangsu University, China

Arata MASUDA, Kyoto Institute of Technology, Japan

Tetsuro MITOMA, Mitsui Chemicals, Inc., Japan

Hiromitsu OHTA, National Fisheries University, Japan

Yelian MIAO, Nanjing University of Technology, China

R.R.Pechon, Agriculture,Bohol Agricultural Promotion Center,Philippines

Zhongyong PAN, Jiangsu University, China

Yimin. SHAO, Chongqing University, China

Noriaki SATONAGA, Showa Denko K.K., Japan

Yukio WATANABE, TOSHIBA CORPORATION, Japan

Toshiaki WAKABAYASHI, Kagawa University, Japan

Taiyong WANG, Tianjin University, China

Shiming WANG, Shanghai Ocean University, China

Hongtao XUE, Jiangsu University, China

Xiaoli XU, Beijing Information Science and Technology University, China

Mitsushi YAMASHITA, Mie University, Japan

Ruqiang YAN, School of Instrument Science and Engineering, China

Yanyang ZI, Xi'an Jiaotong University, China

Chongsheng YUAN, DIAZYME Corporation, USA

Secretariat Board

Email : ijce@nifty.com

(Head) **Hao SUN,** Jiangnan University, China
Email : sunhao@jiangnan.edu.cn

Ke LI, Jiangnan University, China

Feng WANG, Beijing University of Chemical Technology, China

Hongtao XUE, Jiangsu University, China

Haiyang JIANG, MieUniversity, Japan

Liuyang Song, Mie University, Japan

Zhaoyi Guan, MieUniversity, Japan

International Journal of Comprehensive Engineering (IJCE)

International Journal of Comprehensive Engineering (IJCE) is an international interdisciplinary journal that integrates publication from aspects of research on engineering science. This journal provides a medium of communication among engineers and scientists who have engaged in research and development concerning the fields of comprehensive engineering, while maintaining a healthy balance between fundamental and experimental topics. Now, the journal has three separate fields, the scopes of which are Part A: Maintenance Engineering; Part B: Intelligent Engineering; Part C: Engineering in Agriculture, Ocean and Light Industry shown in flows, and other specialized fields will also be updated in the near future.

Part A: Maintenance Engineering

Executive editors：

Prof. Dr. Yanyang ZI
Xi'an Jiaotong University, China
E-mail: ziyy@mail.xjtu.edu.cn

Associate Prof. Dr. Hiromitsu OHTA
National Fisheries University, Japan
E-mail: ohta@fish-u.ac.jp

Prof. Dr. Huaqing WANG
Beijing University of Chemical Technology, China
E-mail: hqwang@mail.buct.edu.cn

Topics of interest for submission on the field of maintenance engineering include, but are not limited to:
Condition Diagnosis Engineering and Technology; Sensing Technology; Maintenance Management; Fault Tolerant System; Fault Self-Recovery Engineering; E-Maintenance; Signal Processing; Risk, Health and Safety Management; Structural Health Monitoring; Information and Communication Technology; Data and Information Fusion; Reliability/Quality; Maintenance Robot; Data Quality and Acquisition; Human Factors; Education and Training; Risk Based Engineering; Others on Maintenance.

Part B: Intelligent Engineering

Executive editors：

Prof. Dr. Huaqing WANG
Beijing University of Chemical Technology, China
E-mail: hqwang@mail.buct.edu.cn

Associate Prof. Dr. Arata MASUDA
Kyoto Institute of Technology, Japan
E-mail: masuda@kit.ac.jp

Associate Prof. Dr. Ke LI
Jiangnan University, China
E-mail: like@jiangnan.edu.cn

Topics of interest for submission on the field of intelligent engineering include, but are not limited to:
Application of Artificial Intelligence in Engineering; Intelligent Design, Modeling, Planning and Control for Applied Engineering; Intelligent Robot System; Intelligent Fault Diagnosis; Intelligent Signal Processing for Applied Engineering; Others on Intelligent Engineering.

Part C: Engineering in Agriculture, Ocean and Light Industry

Executive editors (Agriculture):

Prof. Dr. Hanping MAO
Jiangsu University, China
E-mail: maohp@ujs.edu.cn

Prof. Dr. Jianping HU
Jiangsu University, China
E-mail: hujp@ujs.edu.cn

Executive editor (Ocean):

Prof. Dr. Shiming WANG
Shanghai Ocean University, China
E-mail: smwang@shou.edu.cn

Executive editor (Light Industry):

Prof. Dr. Lixin LU
Jiangnan University, China
E-mail: lulx@jiangnan.edu.cn

Topics of interest for submission on the field of engineering in agriculture, ocean and light industry include, but are not limited to:
Agriculture Engineering: Agricultural Equipment and Mechanical Engineering; Agricultural Bioenvironmental Engineering; Agricultural Renewable Energy Engineering; Agricultural Produce Processing Engineering; Agricultural Information and Electrical Technologies; Others on Agricultural Engineering.
Ocean Engineering: New Ocean Energy; Ocean Maintenance Technology; Ocean Monitoring Technology; Ocean Diagnosis Method; Ocean Experimental Development; Professional Sensor Technology; Observational and Computational Tools Others on Ocean Engineering.
Light Industry Engineering: Agri-food Products Processing/Packaging Technology and Equipment; Comprehensive Utilization of Resource; Preservation; Storage and Packaging of Agri-food Products; Innovative IT Applications in Agri-food Chain; Sensing, Testing, Automation and Internet of Things Technologies; Green Environmental Protection; Energy Saving Technologies; Others on Light Industry.

Manuscript Submission

Manuscripts should be submitted online at http://www.iace-journal.org/ by registering and logging in to the website of the IJCE. Once you have registered, please click the "Submit Manuscript" to go to the submission from. Please use the MS Word template file to prepare your manuscript. Manuscript prepared in MS Word must be converted into a single file before submission. The Microsoft Word template file can be downloaded from the website of the IJCE.

Submission Declaration

The submission, such as articles, reviews, technical report etc., to the IJCE means these facts that the work described has not been published previously, that it is not under consideration for publication elsewhere, that its publication is approved by all authors and tacitly or explicitly by the responsible authorities where the work was carried out, and that, if accepted, it will not be published elsewhere including electronically in the same form, in English or in any other language, without the written consent of the copyright-holder.

Copyright

Authors will be asked to complete a "Copyright Transfer Statement", when submitting the manuscript. Acceptance of the agreement will ensure the widest possible dissemination of information. Permission of the publisher is required for resale or distribution outside the institution and for all other derivative works, including compilations and translations. The "Copyright Transfer Statement" can be downloaded from the website of the IJCE as follows:
http://www.iace-journal.org/views/Copyright_Transfer_Statement.pdf.

Review Policy

The following types of contribution to the IJCE are peer-reviewed: Articles, Reviews and Technical Reports. The articles accepted for publishing in the IJCE include regular paper and letter, which will be decided by editors according the reviewing results. All forms of published correction may also be peer-reviewed at the discretion of the editors. Other contributed types to the IJCE, particularly if they present technical information, may be peer-reviewed at the discretion of the editors. For any general questions and comments about the peer-review process, the journal or its editorial policies that are not mentioned here, please contact us using the email: ijce@nifty.com. Questions about a specific submitted manuscript should be directed to the executive editor who is handling the manuscript.

International Journal of Comprehensive Engineering (IJCE)

Volume 3, Number 1, December 2014 (ISSN 2186-2680)

********** Part A : Maintenance Engineering **********

1 Hailiang Sun, Yanyang Zi, Zhengjia He, Nianhong Wan, Han Liu

Multiwavelet Denoising Using SureBlock Thresholding and Its Application in the Gearbox Fault Diagnosis of Rolling Mills

********** Part B : Intelligent Engineering **********

11 Ke Zhang, Huoqing Zhou, Yukui Zhang, Lixin Gao

Research on Autocorrelation-based Parallel Stochastic Resonance System of Low-speed Heavy-load Equipment

16 Qing Guo, Shengyun Liu, Masaru Noda, Juan Chen

Optimal Grade Transition for Quality Control of Continuous Free Radical Polymerization Process

25 Xianwei Wang, Guanghui Luo, Huaqing Wang, Sheng Bai, Yuxin He

Research on Portable Acoustic Emission Detection System Based on the Windows Program Design

******** Part C : Engineering in Agriculture, Ocean Industry and Light Industry ********

32 Jiuhong Jiang, JinZhi Zhou

The Shock Response Spectrum of two degree-of-freedom-system under the Action of TerminalPeak Sawtooth Pulse

38 Feng Wang, Hongwu Chen, Can Wang, Shuai Zhang, Ting Gao

Fixed Deck Foam Extinguishing System on the Sea

Copyright © 2012 DET Corp., Japan All Rights Reserved
International Journal of Comprehensive Engineering
Part A, 3(1), 1-10, 1
Doi: 14270/IJCE2014.3.1.a1
Regular paper

ISSN 2186-2680
e-ISSN 2186-2656
www.iace-journal.org

Multiwavelet Denoising Using SureBlock Thresholding and Its Application in the Gearbox Fault Diagnosis of Rolling Mills

Hailiang Sun[1], Yanyang Zi [1,#], Zhengjia He [1], Nianhong Wan [2], Han Liu [2]

[1] State Key Laboratory for Manufacturing and Systems Engineering, School of Mechanical Engineering, Xi'an Jiaotong University, 710049, Xi'an, China
[2] Shanghai Baosteel Industry Technological Service Co., Ltd. 201900, Shanghai, China

[#] Corresponding author: ziyy@mail.xjtu.edu.cn; Tel.: +86-29-82666389-604; Fax: +86-29-82663689-605

Abstract: Multiwavelet denoising using SureBlock thresholding is proposed in order to effectively extract weak fault features which are immersed in noises cause by equipment and the surrounding environment. The effect of wavelet block threshold denoising mainly depends on the selection of shrinkage functions and thresholds. Multiwavelets have more than two different multiscaling functions and they possess excellent properties of the orthogonality, symmetry, compact support and high vanishing moments simultaneously. Based on the correlation between multiwavelet coefficients, this paper selects the optimal block length and threshold by using the minimum of Stein's Unbiased Risk Estimate when estimating unknown fault features. The optimal block length and threshold are applied for the effective feature extraction and noise elimination at each decomposition level. The simulation signal validates the effectiveness of the proposed method, and the gearbox fault diagnosis in the rolling mills indicates that the proposed method can successfully extract two local scuffing faults caused by the surface welding at a high temperature on the pinion.

Keywords: Multiwavelet, Block Thresholding, Stein's Unbiased Risk Estimate, Signal Denoising, Fault Diagnosis.

Received: July 12, 2012 / Accepted: Aug. 12, 2013 / Published: Jan. 6, 2014

1. Introduction

Safety and reliability of the rolling mills, which are key equipment in the metallurgy, are essential for the product quality and efficiency. The rolling mills are operating under the complex and harsh conditions such as fatigue, elevated temperature and heavy load for a long term. The kernel parts of the rolling mills, such as the main gearboxes, may inevitably generate various faults or damages. Weak features of incipient faults (the faults in the early stages) are always immersed in noises cause by the equipment and the surrounding environment. The condition monitoring, fault diagnosis and prognosis of incipient faults for key equipment have becoming more and more difficult [1]. Therefore, how to eliminate noises from measured signals and how to enhance useful fault features are critical problems for accurate feature extraction and fault diagnosis. Because of the multi-resolution analysis (MRA) of wavelet transform, wavelet denoising technique has obtained a good result in signal denoising and been widely used in engineering applications [2].

The effect of wavelet denoising mainly depends on the feature extraction and noise elimination. For feature extraction, multiwavelets can possess such properties as compact support, symmetry, orthogonality and high vanishing moment simultaneously, which scalar wavelets cannot possess. Moreover, multiwavelets possess more than two different multiscaling functions and multiwavelet functions, which can effectively match the various fault features caused by the transmission path, the power frequency disturbance or the equipment resonance. Hence, multiwavelets have remarkable advantages over the scalar wavelets in signal denoising, image processing and fault feature extraction [3,4]. For wavelet denoising, Donoho and

Johnstone[2] introduced scalar wavelet threshold to signal denoising and proved its validity. The threshold scheme compared all wavelet coefficients with the chosen threshold and shrunk these coefficients. Visualshrink technique [5] adopted the global threshold $\lambda = \hat{\sigma}\sqrt{2\log N}$ at each wavelet decomposition level, where N was the length of the signal and $\hat{\sigma}$ was the estimated noise variance. Sureshrink method [6] selected the optimal threshold by minimizing the Stein's unbiased risk estimate (SURE) [7], the threshold was data-driven and would lead to a good denoising result. The above-mentioned term-to-term denoising techniques, which neglect the correlation between wavelet coefficients of fault features, cannot accurately extract the fault features of the key equipments.

Based on the correlation between neighboring wavelet coefficients, Efromovich [8] proposed the block threshold denoising for estimating a orthogonal sequence. Donoho and Johnstone [6] and Kerkyacharian [9] discussed the universal block threshold denoising at each decomposition level, which was not spatial adaptive, for the regression analysis and the density estimation. Hall [10] proposed the local block hard-threshold denoising, the block length was $(\log n)^2$ and n was the length of detail coefficients. Cai [11] discussed James-Stein rule for the selection of the block length. The length $\log n$ agreed with the compromise between global and local adaptation. The block threshold denoising was successfully applied to the gear fault diagnosis in the early stage [12], the power quality disturbance [13] and the channel estimation for OFDM system [14].

The result of wavelet denoising using the block threshold mainly depends on the block length and the threshold. However, the conventional block threshold denoising techniques cannot effectively solve the problems: (1) The threshold is selected according to prior experience, which will generate a large deviation in signal denoising. (2) The universal threshold is adopted at all decomposition levels, which is not the optimal one for each level. In order to improve conventional wavelet denoising techniques, Cai [15] estimated the optimal block length and threshold using the minimum of SURE, which is called SureBlock. Further studies are still necessary for the proof of the optimal selection of block lengths and thresholds.

This paper proposed a multiwavelet denoising technique using SureBlock thresholding. The structure of the paper is organized as follows. The introduction of wavelet threshold denoising is given in Section 1. The summary of multiwavelets is introduced in Section 2. In Section 3, the theory of the block threshold and SureBlock is given. In Section 4 and Section 5, the proposed method is applied to the simulation experiment and the gearbox fault diagnosis in the rolling mills. Conclusions are given in Section 6.

2. Summary of multiwavelets

2.1 Multiscaling and multiwavelet functions

Like the scalar wavelets, the theory of multiwavelets is based on MRA [16]. The difference is that multiwavelets are generated by dilations and translations of the vector functions $\boldsymbol{\Phi} = [\phi_1, \phi_2, \cdots, \phi_r]^{\mathrm{T}}$, where $r \in N$ and the space will be

$$V_j = \overline{\operatorname{span}\left\{2^{-j/2}\varphi_i\left(\frac{t}{2^j} - k\right) : 1 \le i \le r, k \in \mathbf{Z}\right\}} \tag{1}$$

The vector functions $\boldsymbol{\Phi}(t)$ and $\boldsymbol{\Psi}(t)$ will satisfy a matrix dilation equation

$$\boldsymbol{\Phi}(t) = \sqrt{2}\sum_{k=0}^{M} \boldsymbol{H}_k \boldsymbol{\Phi}(2t-k) \quad k \in \mathbf{Z} \tag{2}$$

$$\boldsymbol{\Psi}(t) = \sqrt{2}\sum_{k=0}^{M} \boldsymbol{G}_k \boldsymbol{\Phi}(2t-k) \quad k \in \mathbf{Z} \tag{3}$$

The coefficients $\{\boldsymbol{H}_k\}$ and $\{\boldsymbol{G}_k\}$ are $r \times r$ matrices and $\boldsymbol{\Psi} = [\psi_1, \psi_2, \cdots, \psi_r]^{\mathrm{T}}$ are multiwavelet functions corresponding to multiscaling functions $\boldsymbol{\Phi}$. In the frequency domain, Eq. (2) and (3) are expressed as

$$\hat{\boldsymbol{\Phi}}(2\omega) = \mathbf{H}(\omega)\hat{\boldsymbol{\Phi}}(\omega) \tag{4}$$

$$\hat{\boldsymbol{\Psi}}(2\omega) = \boldsymbol{G}(\omega)\hat{\boldsymbol{\Phi}}(\omega) \tag{5}$$

$\boldsymbol{H}(\omega)$ and $\boldsymbol{G}(\omega)$ are the refinement symbols corresponding to $\boldsymbol{\Phi}$ and $\boldsymbol{\Psi}$, respectively.

$$\begin{aligned}\mathbf{H}(\omega) &= \frac{1}{2}\sum_{k=0}^{M}\mathbf{H}_k e^{-i\omega k}\\ \mathbf{G}(\omega) &= \frac{1}{2}\sum_{k=0}^{M}\mathbf{G}_k e^{-i\omega k}\end{aligned} \tag{6}$$

The widely used multiwavelet system was constructed by Geronimo, Hardin and Massopust, named GHM multiwavelets [17]. They have such properties as orthogonality, symmetry, compact support and second approximation order. The multiscaling functions and multiwavelet functions are shown in Fig. 1.

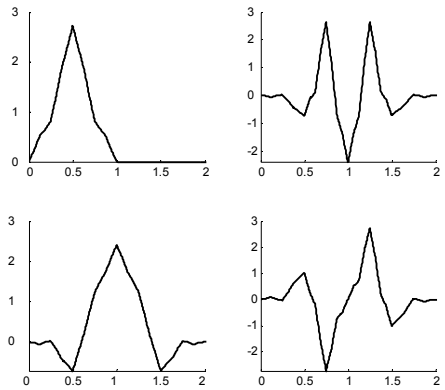

Fig. 1 GHM multiscaling functions and multiwavelet functions

2.2 Multiwavelet transforms and preprocessing

Multiwavelet transforms are analogous to scalar wavelet transform. The difference is that multiwavelets are block convolution and block downsampling and upsampling [18]. With the starting vector coefficients $\boldsymbol{s}_{0,0},\cdots,\boldsymbol{s}_{0,2^j-1}$, the decomposition of multiwavelets is

$$\begin{aligned}\mathbf{s}_{j-1,n} &= \sum_k \mathbf{H}_{k-2n}\mathbf{s}_{j,k}\\ \mathbf{d}_{j-1,n} &= \sum_k \mathbf{G}_{k-2n}\mathbf{s}_{j,k}\end{aligned} \tag{7}$$

Each low frequency coefficients $\boldsymbol{s}_{j-1,n}$ and high frequency coefficients $\boldsymbol{d}_{j-1,n}$ are vectors of r dimension javascript:showjdsw('showjd_1','j_1'). The reconstruction of multiwavelets is

$$\mathbf{s}_{j,k} = \sum_n \mathbf{H}^*_{k-2n}\mathbf{s}_{j-1,n} + \sum_n \mathbf{G}^*_{k-2n}\mathbf{d}_{j-1,n} \tag{8}$$

the superscript * denotes the complex conjugate transpose.

As each multiwavelet system is a matrix-valued multirate filter bank, its input data streams need r dimension rows (in this paper, $r=2$) javascript: showjdsw ('showjd_1','j_1'). Usually there is only one input stream $f[n]$ and so some kind of preprocessing must be done before the implementation of multiwavelet transforms. Correspondingly, a postprocessing is needed to be performed after reconstruction and it must be the inverse process of the preprocessing.

The most obvious way to get the second input row is just to repeat the input stream with a factor α, namely oversampling scheme [19]. The preprocessing is

$$\mathbf{s}_{0,n} = \begin{pmatrix} s_{0,n}^{(0)} \\ s_{0,n}^{(1)} \end{pmatrix} = \begin{pmatrix} f[n] \\ \alpha * f[n] \end{pmatrix} \tag{9}$$

Here α is a constant and makes the system hold approximation order higher than zero. For GHM multiwavelets, $\alpha = 1/\sqrt{2}$. A different way is preprocessing the signal $f[n]$ with a matrix pre-filter Q, called critically sampling scheme. There are various pre-filters with different properties. It has been proved that oversampling representations are better for feature extraction than critically sampling ones [20]. Therefore, oversampling scheme is used as the multiwavelet preprocessing in this paper.

3. Multiwavelet denoising using SureBlock thresholding

3.1 Multiwavelet block threshold denoising

Suppose the measured dynamic signal $s(n)$ is

$$s(n) = f[n] + \sigma r[n] \tag{10}$$

where $r(n)$ are independently distributed as $N(0,1)$, σ is the variance of the distribution, $f[n]$ is the unknown features which we would like to recover. The purpose of signal denoising is to eliminate noises and to recover the unknown features $f[n]$ form the noisy signal $s(n)$.

For multiwavelet denoising techniques, preprocessing is needed to transform the one-stream input signals into multiple-stream ones. Then Eq. (10) can be expressed as $\boldsymbol{S} = \boldsymbol{F} + \boldsymbol{E}$, where $\boldsymbol{S} = \left[s^{(1)}, s^{(2)}\right]^{\mathrm{T}}$ is the sampled vector signal after preprocessing, $\boldsymbol{F}$ is the unknown vector features corresponding to $f[n]$ in the one-stream case, $\boldsymbol{E}$ obeys a multivariate normal distribution $N(0,\boldsymbol{V}_j)$. The matrix $\boldsymbol{V}_j$ is the covariance matrix for the high-frequency multiwavelet coefficients at the resolution scale j. Using the standard transform $\theta_{j,k} = \boldsymbol{D}_{j,k}^{\mathrm{T}} \boldsymbol{V}_j^{-1} \boldsymbol{D}_{j,k}$, we obtain a positive scalar value that in the absence of any signal component will have a χ_M^2 distribution, where M is the number of elements in $\boldsymbol{S}$. It is these $\theta_{j,k}$ values that are thresholded, and the coefficients vectors can then be adapted accordingly.

We can use a robust covariance estimation method to estimate $\boldsymbol{V}_j$ directly from the observed coefficients [16]. The pseudo-code for robust covariance estimation can be listed as follows [21]:

$$\mathrm{mad}(y) = 1.4826 * \mathrm{median}(|y - \mathrm{median}(y)|) \tag{11}$$

float a_1, a_2, b_1, b_2, $\boldsymbol{V}_j$ are

$$\begin{aligned} a_1 &= 1/mad(row_1) \\ a_2 &= 1/mad(row_2) \\ b_1 &= mad(a_1 \cdot row_1 + a_2 \cdot row_2) \\ b_2 &= mad(a_1 \cdot row_1 - a_2 \cdot row_2) \end{aligned} \qquad \boldsymbol{V}_j = \begin{bmatrix} \dfrac{1}{a_1 \cdot a_1} & \dfrac{b_1 - b_2}{(b_1 + b_2) \cdot a_1 \cdot a_2} \\ \dfrac{b_1 - b_2}{(b_1 + b_2) \cdot a_1 \cdot a_2} & \dfrac{1}{a_2 \cdot a_2} \end{bmatrix} \tag{12}$$

In the first row y is a row vector, and the definition of $\mathrm{mad}(y)$ is given. This definition is applied to calculate a_1, a_2, b_1, b_2 by replacing y with row_1 and row_2. Here row_1 and row_2 are the two rows of multiwavelet coefficients at the resolution scale j.

For multiwavelet block threshold denoising, the incorporation of the multiwavelet coefficients of the block k at the resolution scale j is represented as below

$$Sum_{j,k}^2 = \sum_{n=0}^{L} \theta_{j,k+n}^2, \tag{13}$$

where L is the block length.

The shrinkage rule for multiwavelet block threshold denoising is expressed as:

$$\hat{\boldsymbol{D}}_{j,k} = \begin{cases} \boldsymbol{D}_{j,k}(1 - \dfrac{\mu^2}{Sum_{j,k}^2}), & Sum_{j,k}^2 \geq \mu^2 \\ 0, & Sum_{j,k}^2 < \mu^2 \end{cases} \tag{14}$$

where $\mu = 2\log nn$, nn is the length of the multiwavelet coefficients at the scale j.

As mentioned above, the block length and the threshold are two variant parameters which can be optimized in multiwavelet block threshold denoising. Different block lengths are selected at different decomposition levels. As shown in Fig. 2, the block lengths at the decomposition level 1-3 are set to 2, 3 and 1, respectively. For each decomposition level, the suitable threshold can be selected to eliminate much noise and well recover the unknown features.

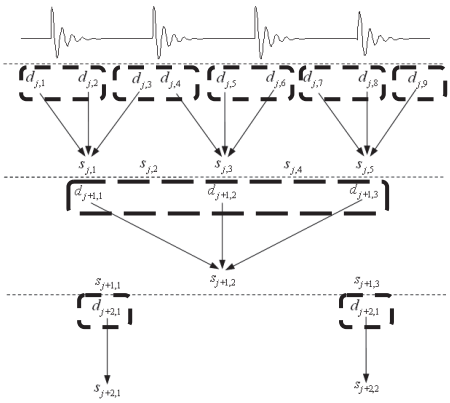

Fig. 2 Multiwavelet denoising based on the block threshold

3.2 Multiwavelet denoising using SureBlock thresholding

SureBlock thresholding chooses the suitable block lengths and the threshold by minimizing SURE. Suppose the multiwavelet coefficients at the subband m are $w_m = \{s_{i,j,k},\ i,j,k \in \text{the } m \text{ subband}\}$, the unknown feature without noise is $f_m = \{f_{i,j,k}\}$, where i denotes the i-th branch of multiwavelet decomposition, j denotes the decomposition level and k denotes the translation of the multiwavelet coefficients at the level j. Stein [7] proved that the expected loss or risk of the estimator $\hat{f}_j$ for the true feature f_j could be unbiased estimated based on the multiwavelet coefficients w_m. Generally, suppose the noise variance is $\sigma = 1$, then we can get

$$E\{\left\|\hat{f}_j - f_j\right\|_2^2\} = N_m + E\{\left\|g(f_j)\right\|_2^2 + 2\nabla g(f_j)\} \tag{15}$$

where $g(f_j) = \{g_n\}_{n=1}^{N_m} = \hat{f}_j - f_j$, $\nabla \bullet g = \sum_n \frac{\partial g_n}{\partial f_j}$, according to Eq. (14), we can get

$$E\left\|g_n(f_n)\right\|_2^2 = \left\|\hat{f}_j - f_j\right\|_2^2 = \begin{cases} \frac{\mu^4}{(Sum_{j,k}^2)^2} f_n^2, & Sum_{j,k}^2 > \mu^2 \\ f_n^2, & Sum_{j,k}^2 \le \mu^2 \end{cases} \tag{16}$$

$$\nabla \frac{\partial g_n}{\partial f_j} = \begin{cases} -\mu^2 \frac{Sum^2{}_{j,k} - 2f^2{}_n}{(Sum_{j,k}^2)^2}, & Sum^2{}_{j,k} > \mu^2 \\ -1, & Sum^2{}_{j,k} \le \mu^2 \end{cases} \tag{17}$$

$$\text{SURE}(w_m, \mu, L) = N_m + \sum_n \left\|g_n(f_n)\right\|_2^2 + 2\sum_n \frac{\partial g_n}{f_n} \tag{18}$$

Then $E\{\left\|\hat{f}_j - f_j\right\|_2^2\} = E\{\text{SURE}(w_m, \mu, L)\}$ is the unbiased estimator of the expected loss. The minimum of $\text{SURE}(w_m, \mu, L)$ can be obtained by selecting the suitable block length L^m and threshold μ^m, that is

$$(\mu^m, L^m) = \arg\min_{\mu,\ L} \text{SURE}(\text{w}_m, \mu, L) \tag{19}$$

As mentioned above, the block length and threshold are calculated by assuming $\sigma = 1$, therefore, for the collected signals with non unit variance, the standard deviation $\hat{\sigma}$ of the signal should be estimated and

the variance of the wavelet coefficients should be normalized. A good estimator for the variance is obtained by the median value of the absolute values of the diagonal sub band coefficients at the finest decomposition level.

$$\hat{\sigma} = \frac{median(|f_j|)}{0.6745} \tag{20}$$

The estimator is constructed through a hybrid method. Set $T_d = nn\sum(x_i^2 - 1)$, $\gamma_d = nn^{-1/2}\log_2^{3/2} nn$ and $\mu^F = 2L\log nn$. (μ^*, L^*) denotes the optimal block length and threshold which have the minimum SURE, under the additional constraint condition in the searching region.

$$(\mu^*, L^*) = \underset{\max\{L-2,\,0\}\le\mu\le\mu^F,\ 1\le L\le nn^{1/2}}{\arg\min} SURE(x, \mu, L) \tag{21}$$

The estimator $\hat{f}^*(x)$ for f is

$$\begin{cases} \widehat{\underline{f}^*}_b = \hat{\underline{f}}_b(\mu^*, L^*) & T_d > \gamma_d \\ \widehat{f^*}_i = (1 - \dfrac{2\log nn}{x_i^2})_+ x_i & T_d \le \gamma_d \end{cases} \tag{22}$$

The estimator is called SureBlock estimator. When $T_d \le \gamma_d$, it degenerates to James-Stein estimator whose block length is 1. The hybrid scheme is used to guard against the situations of extreme sparsity of a mean vector.

As shown in Fig. 3, multiwavelet denoising using SureBlock thresholding can be generalized below.

1) Preprocess the measured signal and perform *l*-level decomposition;
2) Select the optimal block length and threshold by minimizing SURE at each decomposition level;
3) Threshold the detail coefficients at each decomposition level according to Eq. (22) using the optimal block length and threshold, the purified signal $\hat{d}_{j,k}$ is obtained.
4) Reconstruct the purified signal $\hat{d}_{j,k}$ at each decomposition level and the approximation signal to obtain the multi-stream denoising result $\tilde{s}_{0,n}$
5) Postprocess the multi-stream denoising result $\tilde{s}_{0,n}$ to obtain the one-stream result $\hat{x}$.

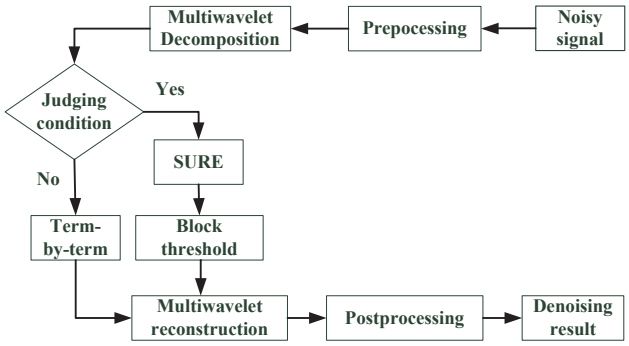

Fig. 3 Multiwavelet denoising using SureBlock thresholding

4. Simulation

To test the effectiveness of the proposed method in this paper, a simulation experiment is designed as follows: Gaussian white noise of large magnitude is added to the periodic impulse signal that is shown in Fig. 4(a), the sampling frequency is 2000Hz. The impulse signal is

$$h(t) = \mathrm{sgn}(t)e^{-200|t|}\sin(2\pi\cdot 600t) \qquad f(t) = \sum_k a * h(t - kT) + n(t) \tag{23}$$

where T denotes the period of the impulse signal, k is a natural number, a denotes the amplitude of the impulse. Moreover, a is used to simulate the randomness in the dynamic signal.

The impulse signal is displayed in Fig. 4(a). In this case, $T = 0.12\text{s}$. The characteristic frequency is 8.33Hz. $h(t)$ represents the defect-induced shock impulses, $n(t)$ represents the noise aroused by other reasons. The simulation signal is shown in Fig. 4(b), the signal has a low signal-to-noise-ratio (SNR), no useful features can be seen in the dynamic signal in time domain. Frequency spectrum is the most common method based on the Fourier transform theory in the frequency domain, which is directly obtained by FFT. Fig. 4(c) shows the frequency spectrum of the simulation signal. There are some spectral lines around 600Hz, which is the decaying frequency of the shock impulses, but the sidebands are not clear.

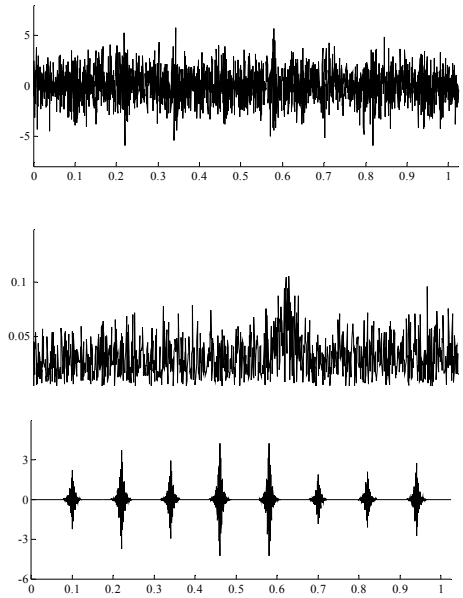

Fig. 4 The simulation signal and its spectrum

GHM multiwavelet denoising using SureBlock gives a distinct result as shown in Fig. 5. Noticeably, the spurious impulses are eliminated and all the features are extracted successfully. The period of the impulses is 0.12s that confirms the validity of the proposed method. GHM multiwavelet denoising methods using conventional block threshold and neighboring coefficients [22] are selected to be compared with the proposed method. These two methods can extract some shock impulses, while eliminate or weaken the weak shock impulses, as shown in the ellipses of the Fig. 6(b) and 6(c), respectively. The obtained results destroy the period of the shock impulses, which will finally lead to an incorrect fault diagnosis conclusion.

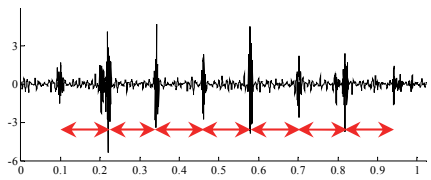

Fig. 5 The result of the proposed method

(a)The result of multiwavelet denoising using the conventional block threshold

(b) The result of multiwavelet denoising using neighboring coefficients

Fig. 6 The result of different multiwavelet denoising techniques

The correlation coefficients and the mean square errors (MSE) between the denoising results and the impulse signal are calculated, as shown in Table 1. The results indicate that multiwavelet denoising using SureBlock has the maximum correlation coefficient and the minimum MSE, which means the proposed method can effectively extract the defect-induced shock impulses and eliminate much noise from the simulation signal.

Table 1 the correlation coefficients and MSE of different multiwavelet denoising techniques.

Multiwavelet denoising techniques	Multiwavelet denoising using SureBlock thresholding	Multiwavelet denoising using the block threshold	Multiwavelet denoising using neighboring coefficients
The correlation coefficients	**0.586**	0.558	0.443
MSE	**0.203**	0.286	0.223

5. Engineering application

The proposed multiwavelet denoising using SureBlock is adopted to the fine rolling mills for a steel strip. In order to verify the proposed method, multiwavelet denoising methods using conventional block threshold and neighboring coefficients are selected to be compared with the proposed method.

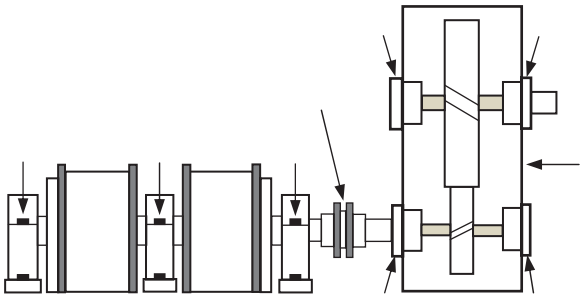

Fig. 7 the gearbox of the rolling mill and the measuring points

As shown in Fig. 7, a fine rolling mill for a hot steel strip are drove by dual motors, The transmission system is a single stage gearbox with a gear ratio of 22/65. The vibration signals are measured at a sampling frequency of 5120 Hz from the measuring points 1~7# on the bearings and the gearbox by using velocity sensors. The rotating frequencies of the pinion and the low-speed shaft are 4.54Hz and 1.54Hz, respectively. As shown in Fig. 8, periodic shock impulses can be vaguely seen in the vibration signal in time domain, the period is 0.22s, which is in accordance with the rotating frequency of the pinion. The local shock impulses are contaminated by the noises of the equipment and the surrounding environment, 100Hz, 497.5Hz and 601.3Hz can be clearly seen in the Fourier spectrum, which are in accordance with the meshing frequency of the gearbox and its harmonics.

GHM multiwavelet denoising using SureBlock is adopted to extract fault features. No notable singular points are detected in the vibration signal except for the shock impulses which occur periodically at an interval of 0.22s. In this study, a five-level multiwavelet decomposition of the vibration signal is first performed after repeated sampling. As shown in Fig. 9, besides the strong impulse cluster I2, there still exist another series of successive impulses I1 submerged in the heavy noise of the original signal. Both of them have a distinct regularity in ranking sequence and magnitude. Each strong impulse I2 and weak impulse I1 emerge alternately and periodically. The periods of shock impulses I1 and I2 are both in accordance with the rotating period of the pinion, indicating that two localized gear teeth faults of the pinion occurred in the gearbox. Furthermore, the time interval between I1 and I2 is close to one third of the pinion's revolution, which means that the two local faults had a distance of one third of the circle.

GHM multiwavelet denoising methods using conventional block threshold and neighboring coefficients are selected to be compared with the proposed method. As shown in Fig. 10(a) and 10(b), multiwavelet denoising using the conventional block threshold can only extract the strong impulses I2, but it cannot reveal the weak impulses I1; multiwavelet denoising using neighboring coefficients can extract the strong impulses I2 and only one weak impulses I1, as shown in the ellipse in Fig. 10(b). Hence, these two methods cannot extract the weak fault features, which will lead to an incorrect fault diagnosis conclusion.

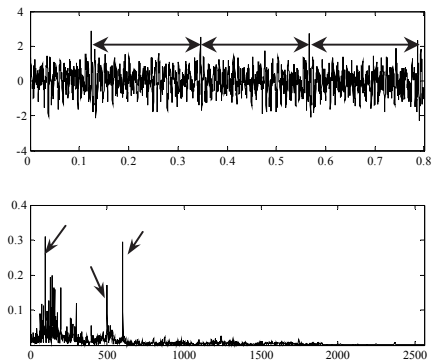

Fig. 8 The vibration signal and its spectrum

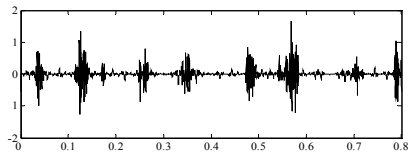

Fig. 9 The denoising result of the proposed method

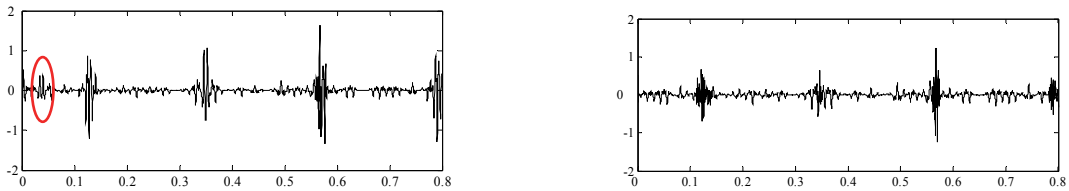

Fig. 10 The result of the vibration signal of the gearbox using different multiwavelet denoising techniques

The field inspection shows that the pinion of the gearbox has two defects, as shown in Fig. 11. The two defects are local scuffing faults caused by surface welding at high temperature, which are about 1/3 of the circle apart. One local scuffing fault is about 1/3 of the teeth, while the other scuffing fault spread along the whole width of the teeth. The fault position and fault severity agree well with the fault diagnostic conclusion.

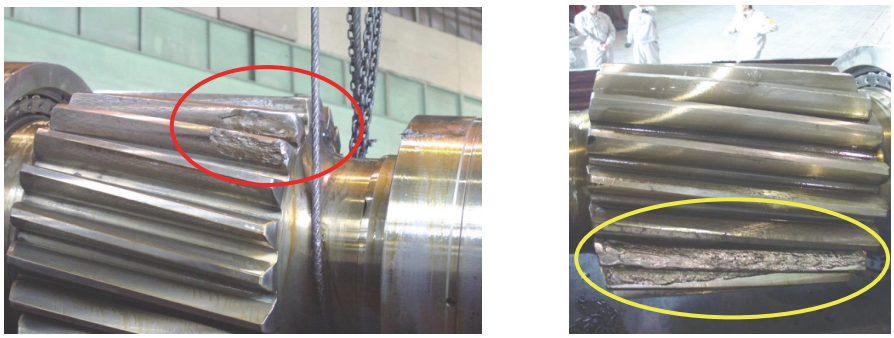

Fig. 11 The defects of the pinion in the gearbox

6. Conclusion

SureBlock thresholding technique calculates the optimal block length and threshold using the minimum of Stein's unbiased risk estimate (SURE) when evaluating unknown features. Multiwavelets possess such properties as orthogonality, compact support, symmetry and high vanishing moment simultaneously, which are important for accurate feature extraction of incipient faults. Moreover, multiwavelets have more than two different basis functions, which can effectively match various fault features caused by the transmission path, the power frequency disturbance or the equipment resonance according to the similarity between wavelet bases and measured signals. Multiwavelet denoising using SureBlock combines the advantages of multiwavelets and SureBlock. The simulation experiment and the fault diagnosis of a gearbox in the rolling mill indicate that the proposed method can effectively extract weak fault features, and accurately diagnose the two local scuffing faults caused by surface welding at high temperature on the pinion.

As mentioned above, the proposed method works well when the noise in the measured signal is Gaussian white noise and the true unknown features are a little stronger than the noises. While in some cases, the

unknown features are relative weak and contaminated by strong background noises and the noises in the measured signal has a complex distribution. It is an interesting and significant research topic to develop based on the proposed method. The authors would like to investigate this topic in the future.

Acknowledgment

This research was financially supported by the project of National Natural Science Foundation of China (No. 50975220, No. 51035007) and National Basic Research Program of China (No. 2009CB724405)

References

[1] J. Yuan, Z. J. He and Y.Y Zi. Gear Fault Detection Using Customized Multiwavelet Lifting Schemes, *Mechanical system and signal processing*, Vol. 24, No. 5, pp. 1509-1528, 2010.

[2] D. L Donoho. De-nosing by Soft-thresholding, *IEEE Transactions on Information Theory*, Vol. 41, No. 3, pp. 613-627, 1995.

[3] V. Strela, P. N. Heller, G. Strang and et al. The Application of Multiwavelet Filterbanks of Image Processing, *IEEE Transactions on Signal Processing*, Vol. 8, No, 4, pp. 548-563, 1999.

[4] S. E. Khadem and M. Rezaee. Development of Vibration Signature Analysis Using Multiwavelets Systems, *Journal of Sound and Vibration*, Vol. 261, No. 4, pp. 613-633, 2003.

[5] D. L Donoho and I. M. Johnstone. Ideal Spatial Adaptation via Wavelet Shrinkage, *Biometrika*, Vol. 81, No. 3, pp. 425-455, 1994.

[6] D. L. Donoho and I. M. Johnstone. Adapting to Unknown Smoothness via Wavelet Shrinkage, *Journal of the American Statistical Association*, Vol. 90, No. 432, pp. 1200-1224, 1995.

[7] C. Stein. Estimation of the Mean of a Multivariate Normal Distribution, *The Annals of Statistics*, Vol. 9, No. 6, pp. 1135-1151, 1981.

[8] S. Y Efromovich. Nonparametric Estimation of a Density of Unknown Smoothness, *Theory of Probability and its Applications*, Vol. 30, pp. 557-568, 1986.

[9] G. Kerkyacharian, D. Picard and K. Tribouley. Lp Adaptive Density Estimation, *Bernoulli*, Vol. 2, No. 3, pp. 229–247, 1996.

[10] P. Hall, G. Kerkyacharian and D. Picard. On the Minimax Optimality of Block Thresholded Wavelet Estimators, *Statistica Sinica*, Vol. 9, pp. 33-50, 1999.

[11] T. Cai. Adaptive Wavelet Estimation: A Block Thresholding and Oracle Inequality Approach, *The Annals of Statistics*, Vol. 27, pp. 898-924, 1999.

[12] Z. X Chen, J. W Xu and D. B Yang. Denoising Method of Block Thresholding Based on DT-CWT and its Application in Mechanical Fault Diagnosis, *Chinese journal of mechanical engineering*, Vol. 43, No. 6, pp. 200-204, 2007 (in Chinese).

[13] Y.L Yang, J. Liu and G. X Zhu. Channel Estimation Based on Block Thresholding Wavelet Denoising for OFDM System, *Computer Science*, 38(6): 74-77, 2011 (in Chinese).

[14] W. Q. Huang and Y. X. Dai. Block-Thresholding Approach for Power Quality Disturbance Denoising, *Transactions of China electro technical society*, Vol. 22, No. 10, pp. 160-166, 2007.

[15] T. Cai and H. Zhou. A Data-Driven Block Thresholding Approach to Wavelet Estimation, *The Annals of Statistics*, Vol. 37, pp. 569-595, 2009.

[16] T. N. T Goodman and S. L Lee. Wavelets of multiplicity τ, *Transactions of the American Mathematical Society*, Vol. 342, pp. 307-324, 1994.

[17] J. S Geronimo, D. P Hardin and P. R Massopust. Fractal Functions and Wavelet Expansions Based on Several Scaling Functions, *Journal of Approximation Theory*, Vol. 78, pp. 373-401, 1994.

[18] F. Keinert. *Wavelets and Multiwavelets*, A CRC Press Company, 2004.

[19] V. Strela, P. N. Heller, G. Strang and et al. The Application of Multiwavelet Filterbanks Of Image Processing, *IEEE Transactions on Image Processing*, Vol. 8, No. 4, pp. 548-563, 1999.

[20] T. R Downie and B. W Silverman. The Discrete Multiple Wavelet Transform and Thresholding Methods, *IEEE Transactions on Signal Processing*, Vol. 46, No. 9, pp. 2558-2561, 1998.

[21] G. Y. Chen and T. D. Bui. Multiwavelet Denoising Using Neighboring Coefficients, *IEEE Signal Processing Letter*, Vol. 10, pp. 211-214, 2003.

[22] T. T. Cai and B. W. Silverman. Incorporating Information on Neighbouring Coefficients into Wavelet Estimation, *The Indian Journal of Statistics (Series B, Part 2)*, Vol. 63, No. 2, pp. 127-148, 2001.

Copyright © 2012 DET Corp., Japan All Rights Reserved
International Journal of Comprehensive Engineering
Part B, 3(1), 11-15, 2014
Doi: 10.14270/IJCE2014.3.1.b11
Regular paper

ISSN 2186-2680
e-ISSN 2186-2656
www.iace-journal.org

Research on Autocorrelation-based Parallel Stochastic Resonance System of Low-speed Heavy-load Equipment

Ke Zhang [1,#], Huoqing Zhou [2], Yukui Zhang [2], Lixin Gao [1]

[1] S Beijing Key Laboratory of Advanced Manufacturing Technology in BJUT，Beijing, 100124, China
[2] Wuhan Iron and Steel Company Iron Mill, Wuhan, Hubei 430083, China

[#] Corresponding author: kedeai@126.com

Abstract: This paper intends to combine the theory of parallel stochastic resonance and auto correlation approach in simulation data of low-speed heavy-load equipment to improve SNR of the stochastic resonance (SR) system. By analyzing simulation signal and test signal from lab table, it is found that the time cycle and frequency characteristics become more apparent. Such combination enables higher detectivity of SR toward weak signal of low-speed heavy-load equipment fault.

Keywords: Parallel Stochastic Rresonance, Autocorrelation, Weak Signal Detection.

Received: *May 25, 2012 / Accepted: Aug. 12, 2013 / Published: Jan. 6, 2014*

1. Introduction

Currently, a lot of research and application fields show concern to weak signal measurement, aiming to achieve wanted signal extraction from noise. Of several detecting methods, attention is all paid to how to reduce noise while neglecting the damage or suppression to measured signal at the same time by detection system. Parallel SR, on the contrary, intends to enhance weak signal by fully utilizing noise, hoping to identify it by raising SNR. Processed by SR, signal energy will be concentrated at LF whereas HF is suppressed to increase the original SNR. Then extract the fault periodic signal for autocorrelation processing. In such case, it is more accurate to acquire signal characteristics, for the spectrum is more steep, hence making it easier to identify weak signal. By analyzing simulation data and test signal from lab table, it is found that correlation analysis can effectively enhance output SNR of SR[1].

2. Multi-layer auto-correlative SR system

SR phenomenon [2] refers to enhancement of output signal SNR by increasing noise in certain conditions when signal under noise passing Bi-stable system. As for approximation of SR phenomenon, see Langevin equation and figure 1 below:

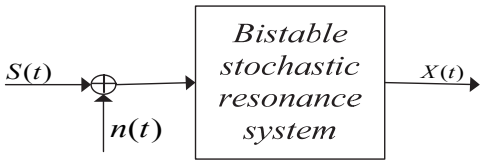

Fig. 1 Stochastic resonance system

$$\frac{dx}{dt} = ax - bx^3 + A\cos(2\pi ft) + n(t) \tag{1}$$

Where: $s(t) = A\cos(2\pi ft)$ is the measured weak periodic signal, $n(t)$ refers to white gaussian noise while satisfying statistical average $E[n(t)] = 0, \mathrm{E}[n(t)n(t+\tau)] = 2\mathrm{D}\delta(\mathrm{t}-\tau)$. Where D is noise intensity, NV is $\sqrt{2\mathrm{D}}$, τ is time delay and $\frac{dx}{dt} = ax - bx^3$ is called as barrier function; a and b are nonlinear system parameters; $X(t)$ is bi-stable system output signal. Figure 1 shows that output signal $X(t)$ presents stochastic resonance phenomenon co-acted by input signal $S(t)$ and noise $n(t)$. Considering the differential equation does not have exact solution, fourth-order Runge-Kutta[3,4] is applied in this paper to work out equation 1.

Taking advantage of the periodicity of signal and randomness of noise, autocorrelation aims to remove noise through autocorrelation calculation. Since signal and noise are independent, signal is only related to itself while there is no relation between noises. Therefore, enhancement of signal SNR can be realized through autocorrelation [5]. Set input signal as follows:

$$y(t) = s(t) + n(t) = A\cos(\omega t + \varphi) + n(t) \tag{2}$$

Its autocorrelation function is:

$$\begin{aligned} R_Y(\tau) &= E[y(\tau)\cdot y(t+\tau)] \\ &= R_S(\tau) + E[s(t)\cdot n(t+\tau)] + E[s(t+\tau)\cdot n(t)] + R_N(\tau) \end{aligned} \tag{3}$$

In terms of ergodicity process, stochastic process autocorrelation function can be replaced by that of time, which is then expressed as:

$$R_X(\tau) = \lim_{T\to\infty}\frac{1}{T}\int_0^T x(t)x(t+\tau)dt \tag{4}$$

In view of limited actual observing time T, the following equation is applied in actual measurement for relevant calculation:

$$R_X(\tau) \cong \hat{R}_X(\tau) = \frac{1}{T-\tau}\int_0^{T-\tau} x(t)x(t+\tau)dt \tag{5}$$

Auto-correlative parallel SR system

When output signal and noise enter into no.1 layer of SR system, output signal will be issued upon SR phenomenon; is issued likewise in no.2 layer. By SR principle, in case input exceeds the critical value, the system will start periodic motion per signal frequency in potential inter-well of bi-stable system. The different parameters of two SR systems have diverse transition critical value (transition difficulty), consequently, output signals and will present phase difference, although the SNR of output signal has improved by two parallel SR systems. Autocorrelation processing can keep periodicity of the signal while remove phase data to achieve zero phase difference between the two output signals and further enhance SNR of them. Upon such processing, time domain averaging can be applied by superposition to get (the output of the whole parallel SR system). Inhibitory action toward noise and enhancement of effective signal acting by parallel SR system then is further promoted. Figure 2 illustrates the principle for auto-correlative parallel SR.

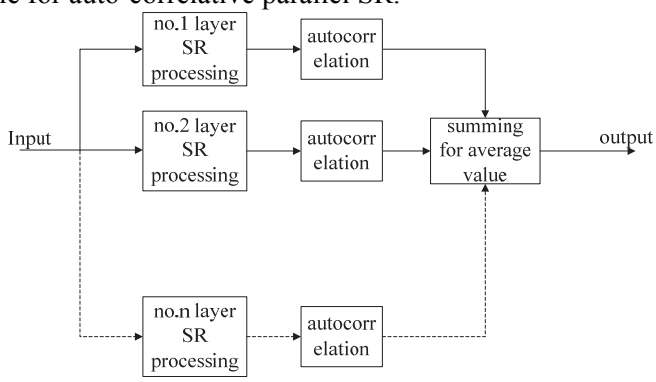

Fig. 2 Auto Correlation parallel stochastic resonance

3. Analysis on simulation data and experimental results

Simulation example proves the effectiveness of parallel SR system, which applies four-layer, with input signal of $S(t)=0.4\cos(2\pi 110t)+0.5\sin(2\pi 60t)+n(t)$, sampling frequency $10000Hz$, sampling points 8192 and noise intensity $D=20$. See Figure 3 for the time wave of original signal. In the parallel SR system, the parameters of system 1, 2, 3 and 4 are $h=1/12, a=0.01, b=1$, $h=1/12, a=0.05, b=1$, $h=1/8, a=0.01, b=1$, $h=1/8, a=0.05, b=1$ respectively. Figure 4 and Figure 5 present time wave and spectrum of output signal for each subsystem of parallel SR while Figure 6 presents that of the whole parallel SR system.

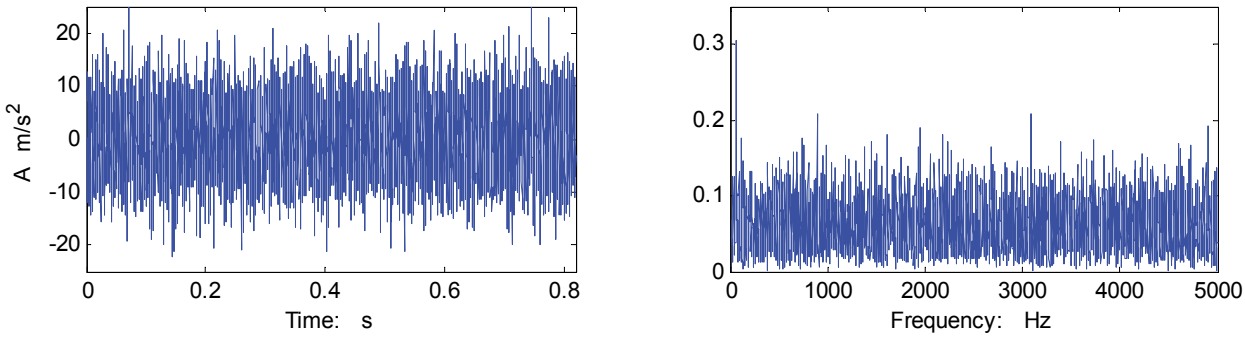

a) Time wave b) Frequency spectrum

Fig. 3 Time wave and Frequency spectrum of input signal

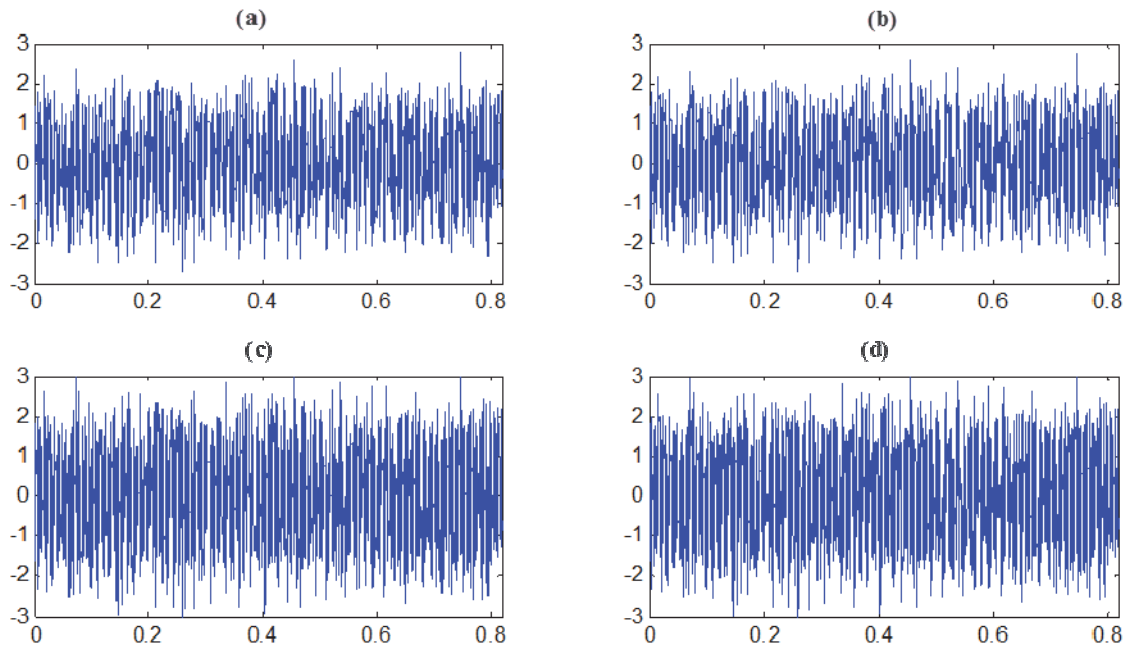

a) No.1 layer of stochastic resonance output time wave
b) No.2 layer of stochastic resonance output time wave
c) No.3 layer of stochastic resonance output time wave
d) No.4 layer of stochastic resonance output time wave

Fig. 4 each layer of stochastic resonance output time wave

Seen from Figure 3, $60Hz$ periodic signal can be acquired upon FT while that of $110Hz$ cannot be identified; by Figure 4 and 5, upon enhancement of SNR and suppression of HF through SR processing, periodic signal $110Hz$ can be vaguely distinguished; in Figure 6, compared with single-layer SR system, the HF noise of original signal has been largely reduced while LF has been highlighted via parallel SR system.

Originally, $110Hz$ frequency spectrum in output signal of parallel SR subsystem (single-layer SR system) is not obvious, upon superposition averaging by autocorrelation, periodicity of $60Hz$ becomes more visible and $110Hz$ takes up the second high point in the frequency spectrum. Moreover, suppression action on HF noise of parallel SR system output has been strengthened and effectively enhances the identification accuracy toward signal SNR and characteristic signal.

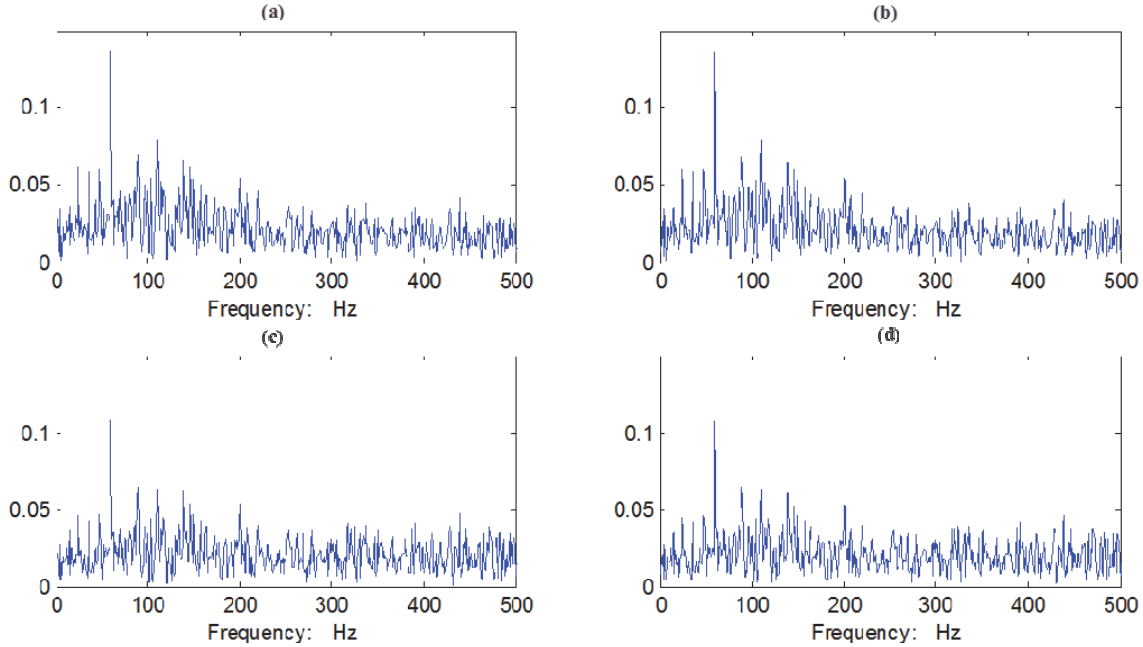

a) No.1 layer of stochastic resonance output Frequency spectrum
b) No.2 layer of stochastic resonance output Frequency spectrum
c) No.3 layer of stochastic resonance output Frequency spectrum
d) No.4 layer of stochastic resonance output Frequency spectrum

Fig. 5 each layer of stochastic resonance output Frequency spectrum

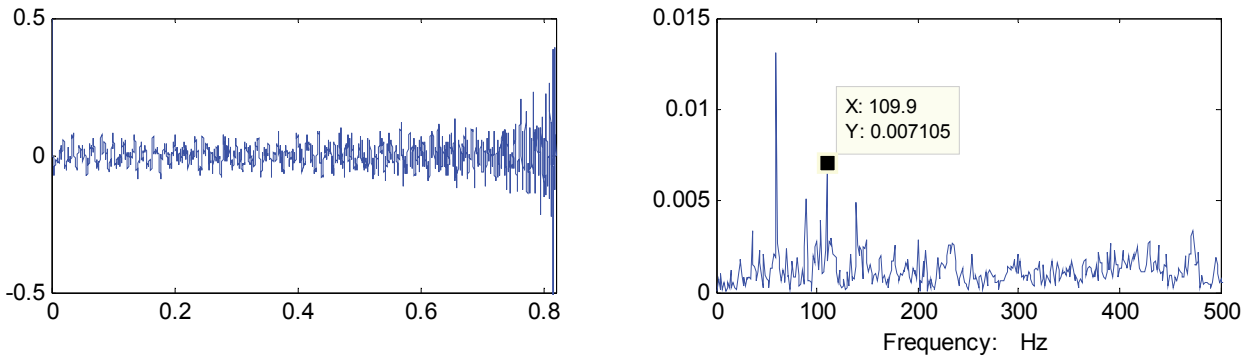

a) Time wave b) Frequency spectrum

Fig. 6 the final output of parallel stochastic resonance

4. Conclusion

This paper proposes autocorrelation-based parallel SR signal processing approach, which adds autocorrelation theory into SR. By theory, the enhancement of signal SNR through such approach is proven; by analysis on simulation experiment and actual measurement data, effectiveness for weak signal detection is proven.

References

[1] R. Benzi, A. Stuera and A. Vulpiani. The mechanism of stochastic resonance, *Journal of Physics A: mathematical and general*, Vol.14, No. 5, pp. 453-457, 1981.

[2] L. Y Gang and T. Y Wang. Power Spectrum Research of Twice Sampling stochastic Resonance Response in A Bistable System, *Physica Sinica*, Vol. 53, No. 3, pp. 717-72, 2004.

[3] L. Y Gang and T. Y Wang. Numerical Research of Twice Sampling Stochastic Resonance for the Detection of a Weak Signal Submerged in a Heavy Noise, *Physica Sinica*, Vol. 52, No. 10, pp. 2432-2437, 2003.
[4] Q. Li and T.Y Wang. Weak Signal Detection Based on Step-Changed Stochastic Resonance, *Journal of Tianjin University*, Vol. 39, No. 4, pp. 432-437, 2006.
[5] Y. B Li and X. Yue. Estimation of Sinusoidal Parameters in Powerful Noise by Multi_layer Autocorrelation, *Journal of Harbin Engineering University*, Vol. 25 ,No. 4, pp. 525-528, 2004.

Copyright © 2012 DET Corp., Japan All Rights Reserved
International Journal of Comprehensive Engineering
Part B, 3(1), 16-24, 2014
Doi: 10.14270/IJCE2014.3.1.b16
Regular paper

ISSN 2186-2680
e-ISSN 2186-2656
www.iace-journal.org

Optimal Grade Transition for Quality Control of Continuous Free Radical Polymerization Process

Qing Guo [1,#], Shengyun Liu [1], Masaru Noda [2] and Juan Chen [1]

[1] College of Information Science and Technology, Beijing University of Chemical Technology, Beijing, 100029, China
[2] Graduate School of Information Science, Nara Institute of Science and Technology, Nara 630-0192, Japan

[#] Corresponding author: guoqing@mail.buct.edu.cn; Tel.: +86-10-6443-4931; Fax: +86-10-6443-7805

Abstract: An optimal grade transition policy is essential when several grades of polymers are produced in the same continuous stirred tank reactor (CSTR). We discuss an optimal grade transition to minimize the amount of raw material assumption during the transition operation as well as to shorten the transition time. Through case study of a free radical styrene polymerization in a pilot CSTR, we show that a combination of regulatory control and dynamic optimization is very effective for the optimal grade transition operation of continuous polymerization reactor.

Keywords: Polymer Quality Control, CSTR, Dynamic Optimization, Grade Transition.

Received: *May 30, 2012 / Accepted: Aug. 12, 2013 / Published: Jan. 6, 2014*

1. Introduction

A grade transition operation is essential in continuous polymerization plants because many grades of polymers are produced from the same reactor. Transitions between different grades result in the production of a considerable amount of off-specification polymer. Flexible operation of the plants depends not only on a steady-state operation but also on an effective grade transition. From the economical viewpoint, reducing the amount of off-specification polymer during the grade transition operation as well as shortening the transition time is important for operating a continuous polymerization reactor.

Dynamic optimization is implemented commonly to achieve optimal grade transition operation [1, 2]. Lee *et al*. [3] proposed a modified differential evolution algorithm for dynamic optimization of a continuous methyl methacrylate-vinyl acetate copolymerization reactor. The object was to determine the optimal trajectories of the control inputs that minimize the transition time. Wei *et al*. [4] applied iterative dynamic programming to the two-grades transition operation in industrial continuous polymerization process. The objective function was presented using polymer properties, including melt index and polymer density.

A well designed control system is important to track the optimally determined dynamic trajectories in the presence of process disturbances and model uncertainties. Several authors combined grade transition optimization with process control [5, 6, 7]. Wang *et al*. [5] developed a nonlinear control system integrating an off-line optimizer and a nonlinear model predictive control to perform optimal grade transition operation at industrial polyolefin reactors. The optimal trajectories of both output and input were calculated off-line using the control vector parameterization (CVP) method with nonlinear first principles models. The derived optimal input sequence was used as a feed-forward signal during grade transition control. Ben Amor et al. [6] applied NLMPC algorithm to the polymer grade transition control using an industrial real-time optimization package. Two simulated polymerization cases were studied. In the continuous methyl methacrylate (MMA) process, the number-average molecular weight (M_n) is controlled by manipulating volumetric flow rate of initiator. The second case of a gas-phase polyethylene reactor was studied as an application of their algorithm to

multiple-input multiple-output control system.

Some researches considered grade transition from other views [8, 9, 10, 11]. Yi *et al*. [8] developed a grade transition strategy for an industrial slurry-phase high-density polyethylene plant from a plant-wide viewpoint. In addition to reactors, models of downstream processes were also included in the optimization. The polymer slurry melt index from the reactors and the polymer pellet melt index from the pelletizer in the plant were used as the properties for grade specification. Asteasuain *et al.*[9] applied a mixed-integer dynamic optimization approach to the simultaneous design and control of a continuous styrene polymerization process. The steady-state operation and grade transition policies have been determined so as to minimize capital and steady-state operating costs as well as off-specification products during grade transition.

Guo *et al.* [12, 13] discussed an optimal steady-state operating condition to produce polymers with the best match to the specified molecular weight distribution (MWD) profile. The MWD profile is characterized by three parameters: the number-average molecular weight (M_n), weight-average molecular weight (M_w), and polydispersity index (*PDI*). Through a study of typical types of free radical polymerization, Guo *et al.* found that an operating condition can be determined by specifying two MWD parameters, M_n and *PDI*, when the termination by combination reaction is included. However, the simultaneous specification of M_n and *PDI* cannot determine an operating condition when the termination reaction by combination is not included. In this case, another parameter should be specified to determine an operating condition.

We discuss an optimal grade transition to minimize the amount of raw material consumption during the transition operation as well as to shorten the transition time in this work. We propose a combination of the regulatory control system and dynamic optimization. Off-line dynamic optimization is carried out to generate the optimal transition trajectory for manipulated variables in the presence of constraints on manipulated, controlled, and state variables.

2. Control System For Optimal Grade Transition

In this section, we consider the optimal polymer production in a pilot-plant continuous stirred tank reactor (CSTR), shown in Fig. 1. The feed streams are composed of the monomer and initiator streams, and these feed streams are well mixed with a solvent before being fed into the reactor. Cooling water is used to remove the heat generated by the polymerization.

The control scheme of an optimal polymer production system for CSTR is also shown in Fig. 1. The polymer grade specification is defined as M_n and *PDI*, which must be satisfied at both steady states. The flow rate of initiator and coolant, F_i and F_j, are selected as manipulated variables. The operating condition specification is defined as the reactor temperature T and the monomer feed ratio α, defined as

$$\alpha = \frac{F_m}{F_m + F_i} \tag{1}$$

where F_m is the flow rates of monomer.

Traditionally gel permeation chromatography (GPC) or size-exclusion chromatography (SEC) have been used to determine polymer MWD [14]. These measurement methods, however, are rather time consuming and virtually impossible to be used in on line control system. For on line purposes, the viscosity and Melt Index measures have been used as a substitute for MWD in online control [15]. In industrial practice, the operators usually operate the polymerization instrument during grade transition and judge the termination of the grade transition operation depending heavily on polymer MWD measured off line in laboratory and their knowledge of experience. The transition time is very long and therefore significant off-specification product is generated.

In this study, two MWD parameters, M_n and *PDI*, are selected to describe polymer grade, which are detected by soft measurement on simulation. When the target polymer quality grade M_n^* and PDI^* are specified, the following two-step approach is adapted to implement the optimal grade transition operation in CSTR.

1) The target operating condition is determined by off-line optimization on basis of the steady-state mathematical model. The objective function is formulated to satisfy the polymer quality specifications.
2) The optimal transition trajectories of input variables are determined by off-line dynamic optimization system using the mathematical model in the presence of constraints on input, output and state variables. With the calculated optimal trajectories of manipulated variables used as the set point signals, the feed-forward controllers drive the polymerization process from the steady state of initial grade to a new steady state that satisfies the target grade specifications.

When both input and output variables satisfy the target requirements for operating condition and polymer quality specification, and the state variables access a quasi-steady state, the grade transition operation is

completed. The regulatory control system is then used in the online implementation of routine operation to account for model errors as well as immeasurable disturbances.

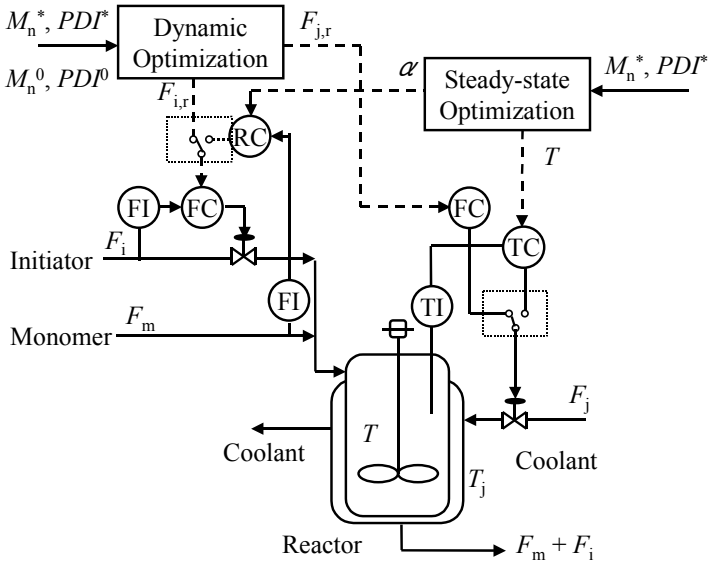

Fig. 1 Control scheme for optimal grade transition in CSTR

3. Dynamic Optimization Method

A general formulation of the optimal grade transition problem is as follows.

$$\min_{u(t),t_f} J(x(t),t_f) \tag{2}$$

$$\text{s.t.} \quad \dot{x}(t) = f(x(t),u(t)), \quad x(t_0) = x_0 \tag{3}$$

$$y(t) = g(x(t),u(t)) \tag{4}$$

$$u^{\min} \le u(t) \le u^{\max} \tag{5}$$

$$y^{\min} \le y(t) \le y^{\max} \tag{6}$$

$$x^{\min} \le x(t) \le x^{\max} \tag{7}$$

Here, $x(t)$ denotes the vector of state variables with the initial conditions x_0 at the start time t_0. $u(t)$ and $y(t)$ denote the vectors of manipulated and controlled variables, respectively. Eqs. (3) and (4) represent the polymerization process model, which is given in the form of differential and algebraic equations. Eqs. (5), (6), and (7) denote the lower and upper bounds on the manipulated, controlled, and state variables, respectively.

Two objective functions are formulated to determine the optimal transition trajectory of manipulated variables, *i.e.* the initiator flow rate F_i and coolant flow rate F_j. The objective function J_1 given by Eq. (8) aims to minimize the transition time $t_{f,1}$.

$$J_1 = t_{f,1} \tag{8}$$

The objective function J_2, given by Eq. (9), focuses on the cost performance of the polymerization process by minimizing the amount of initiator consumption during the polymer grade transition.

$$J_2 = \int_0^{t_{f,2}} F_i(t)dt \tag{9}$$

Based on the minimum transition time $t_{f,1}$ obtained from J_1, the time horizon of J_2, $t_{f,2}$ is specified for handling the optimization problem, *i.e.*, $t_{f,2} = kt_{f,1}$ ($k > 1$), where k is a parameter.

The gPROMS™ [16] is used for the modeling, simulation and dynamic optimization of the continuous free radical polymerization process. In the gPROMS™, there are two standard mathematical solvers available for solving dynamic optimization problems. Both are based on a control vector parameterization (CVP) approach which assumes that the time varying control intervals are piecewise constant (or piecewise linear) functions of time over a specified number of control intervals. The first solver implements a single-shooting dynamic optimization which is more suited to solving problems with many state variables but relatively few control variables and intervals. The second solver implements CVP technique via multiple shooting algorithm. In this work, the dynamic optimization problem is converted to a standard nonlinear programming problem using CVP and is then solved by the latter optimization solver.

4. Mathematical Model of Free Radical Polymerization in CSTR

A mathematical model was developed to simulate the free radical polymerization in CSTR. It is assumed that the flow rate of the product, F, is the same as the total flow rate of the feed, *i.e.*, $F = F_m + F_i$, where F_m and F_i are the flow rates of the monomer and initiator, respectively. The total volume of all reactants in the reactor, V, is assumed to be constant. The monomer and initiator, well mixed with the solvent, are fed into the reactor. I^0 and M^0 are the concentrations of initiator and monomer in the feed mixture, respectively.

The free radical polymerization generally includes the following elementary reactions:

1) Initiation: $I \xrightarrow{K_d} 2R^+$

$R^+ + M \xrightarrow{K_i} R_1$

2) Propagation: $R_j + M \xrightarrow{K_p} R_{j+1}$

3) Transfer to monomer: $R_j + M \xrightarrow{K_{trm}} P_j + R_1$

4) Transfer to solvent: $R_j + S \xrightarrow{K_{trs}} P_j + R_1$

5) Termination by combination: $R_j + R_i \xrightarrow{K_{tc}} P_{j+i}$

6) Termination by disproportionation: $R_j + R_i \xrightarrow{K_{td}} P_j + P_i$

Here, I is the initiator, M is the monomer, and S is the solvent. R^+ is the primary radical; R_j and P_j are the live and dead polymers with chain length j, respectively. K_d, K_i, K_p, K_{trm}, K_{trs}, K_{tc}, and K_{td} are the reaction rate coefficients. All these coefficients are assumed to satisfy the Arrhenius equation, $K = A\exp(-E/R'T)$, where R' is the gas constant.

When one denotes the total concentration of the live polymers as $R = \sum_{j=1}^{\infty} R_j$ and the total concentration of the dead polymers as $P = \sum_{j=2}^{\infty} P_j$, the concentrations of the reaction species are expressed using the following mass balance equations [17].

$$\frac{dI}{dt} = (I^0 - I)/\theta - K_d I \tag{10}$$

$$\frac{dM}{dt} = (M^0 - M)/\theta - 2K_i I - (K_p + K_{trm})MR \tag{11}$$

$$\frac{dS}{dt} = (S^0 - S)/\theta - K_{trs} SR \tag{12}$$

$$\frac{dR}{dt} = -R/\theta + 2K_i I - (K_{tc} + K_{td})R^2 \tag{13}$$

$$\frac{dP}{dt} = -P/\theta + (K_{\mathrm{trm}}M + K_{\mathrm{trs}}S)R + (\frac{K_{\mathrm{tc}}}{2} + K_{\mathrm{td}})R^2 \tag{14}$$

Here, $\theta = V/F$ is the average residential time of the reactant in the CSTR.

The temperatures of the reactor and jacket are described using the following energy balance equations.

$$\frac{dT}{dt} = \frac{F}{V}(T_{\mathrm{f}} - T) + \frac{-\Delta H_{\mathrm{r}}}{\rho C\mathrm{p}} K_{\mathrm{p}} M U_0 - \frac{U_{\mathrm{r}} A_{\mathrm{r}}}{\rho C\mathrm{p} V}(T - T_{\mathrm{j}}) \tag{15}$$

$$\frac{dT_{\mathrm{j}}}{dt} = \frac{F_{\mathrm{j}}}{V_{\mathrm{j}}}(T_{\mathrm{jf}} - T_{\mathrm{j}}) + \frac{U_{\mathrm{r}} A_{\mathrm{r}}}{\rho_{\mathrm{j}} C\mathrm{p}_{\mathrm{j}} V_{\mathrm{j}}}(T - T_{\mathrm{j}}) \tag{16}$$

Here, ΔH_{r}, U_{r}, and A_{r} denote the heat of polymerization, the overall heat transfer coefficient, and the heat transfer area, respectively. F_{j} is the flow rate of coolant, and T_{jf} and T_{j} are respectively the inlet temperatures of coolant and the jacket temperature. T_{f} is the temperature of the feed stream.

The method of moments is used to calculate the MWD parameters, *i.e.*, the number-average molecular weight (M_{n}), weight-average molecular weight (M_{w}), and polydispersity index (*PDI*). The molecular weight distribution moments for the dead polymer are defined as follows:

$$Z_m = \sum_{j=2}^{+\infty} j^m P_j, m = 0,1,2,\cdots \tag{17}$$

Here, Z_m is the mth moment of dead polymer concentrations. M_{n}, M_{w}, and *PDI* are thus calculated by using the dead polymer moments as follows.

$$M_{\mathrm{n}} = M_{\mathrm{m}} Z_1 / Z_0 \tag{18}$$

$$M_{\mathrm{w}} = M_{\mathrm{m}} Z_2 / Z_1 \tag{19}$$

$$PDI = M_{\mathrm{w}} / M_{\mathrm{n}} = \frac{Z_0 Z_2}{Z_1^2} \tag{20}$$

Here, M_{m} is the molecular weight of the monomer.

5. Case Study

5.1 Problem statement

The free radical styrene polymerization process was focused on a case study of the optimal grade transition operation between two polymer grades. Azobisisobutyronitrile and toluene were used as the initiator and the solvent, respectively. The physical properties and kinetic parameters listed in Table 1 are referred from the literatures shown in the footnote.

The initial grade specification is $M_{\mathrm{n}} = 26935$ and $PDI = 1.555$. The target polymer grade specification is $M_{\mathrm{n}}^* = 35700$ and $PDI^* = 1.566$. The operating condition (T and α) is determined by the steady-state optimization [12]. The operating conditions for the initial and target polymer grades are summarized in Table 2.

Bounds of the manipulated variables, F_{i} and F_{j}, and state variables, T and T_{j}, are summarized in Table 3. These constraints must be satisfied during the transition operation including initial and final steady-states.

5.2 Results and discussion

We first determined the shortest transition time $t_{\mathrm{f},1}$ by minimizing the objective function J_1. The shortest transition time was 717 min. Then, we minimized the amount of initiator consumption under the transition time $t_{\mathrm{f},2}$ of 730 min. The optimal trajectories of manipulated variable are shown in Figs. 2 and 3, where both optimal trajectories S_1 and S_2, which minimize J_1 and J_2, are illustrated by solid and dashed lines respectively with S_3, which is described later. Nineteen control intervals were selected in the CVP method. The optimized F_{i} and F_{j} are used as inputs of the feed-forward control system from $t = 0$ to $t = t_{\mathrm{f},1}$ or from $t = 0$ to $t = t_{\mathrm{f},2}$, respectively. After $t = t_{\mathrm{f},1}$ or $t_{\mathrm{f},2}$, the two regulatory controllers come into operation, and the set points are fixed at the target operating condition, *i.e.*, $\alpha = 0.645$ and $T = 354$ K. Then F_{i} and F_{j} are the outputs of the regulatory controller.

As an un-optimized naïve grade transition operation, we changed stepwise both the set points of the two regulatory controllers from the initial operating condition to the target operating condition. This system is called S_3 with practical PID controllers. Figs. 2 and 3 show the results of S_3 by the dotted line.

Table 1 Parameters of styrene polymerization model

K_d / L·mol^{-1}·min^{-1}	$9.48\times10^{16}\exp(-30798.5/1.987T)$ [a]
K_i / L·mol^{-1}·min^{-1}	$0.6K_d$ [a]
K_p / L·mol^{-1}·min^{-1}	$6.306\times10^{8}\exp(-7067.8/1.987T)$ [a]
K_{trm} / L·mol^{-1}·min^{-1}	$7.116\times10^{8}\exp(-12671.1/1.987T)$ [a]
K_{trs} / L·mol^{-1}·min^{-1}	0
K_{tc} / L·mol^{-1}·min^{-1}	$7.5\times10^{10}\exp(-1680/1.987T)$ [a]
K_{td} / L·mol^{-1}·min^{-1}	0
M_m / g·mol^{-1}	100.12
ρCp / cal·L^{-1}·K^{-1}	360.23 [b]
$\rho_i Cp_i$ / cal·L^{-1}·K^{-1}	966.92 [b]
$-\Delta Hr$ / cal·mol^{-1}	16710.77 [b]
U_r / cal·min^{-1}·K^{-1}·m^{-2}	2868 [c]
A_r / m^2	0.11
M^{00} / mol·L^{-1}	4.8
I^{00} / mol·L^{-1}	0.0106
F_m / L·min^{-1}	0.02
T_f / K	350
T_{if} / K	293.2
V / L	3.927
V_i / L	4.318

[a]Yoo *et al*. [18], [b]Asteasuain *et al*. [9], [c]Padhiyar *et al*. [1]

Table 2 Operating conditions for initial and target polymer grades

Variable	Initial values	Target values
α	0.570	0.645
T / K	359.5	354

Table 3 Bounds of manipulated and state variables

Variable	Lower bound	Upper bound
T / K	340	370
T_j / K	275	368
F_i / L·min^{-1}	0.002	0.050
F_j / L·min^{-1}	0.001	0.010

Simulation study is carried out to verify the optimization results. The trajectory in the M_n and PDI space is shown in Fig. 4. The resultant trajectories of operating condition variables, α and T, for the three systems are shown in Figs. 5 and 6. The simulation results of the control system with the three different set-point profiles, S_1

– S_3, are summarized in Table 4. It is shown that all the control systems finally reached the target specification in the M_n and *PDI* space. For S_1 and S_2, the termination time were the final transition time $t_{f,1}$ and $t_{f,2}$ respectively. In case of system S_3, however, the termination time was about 1000 min, which is much longer than that of system S_1 and S_2. The amount of initiator consumption of system S_3 was also much larger than that of system S_1 and S_2. This means that two systems with the combination of dynamic optimization and regulatory controllers, S_1 and S_2, are superior to the non-optimized naïve PID control system for grade transition operation.

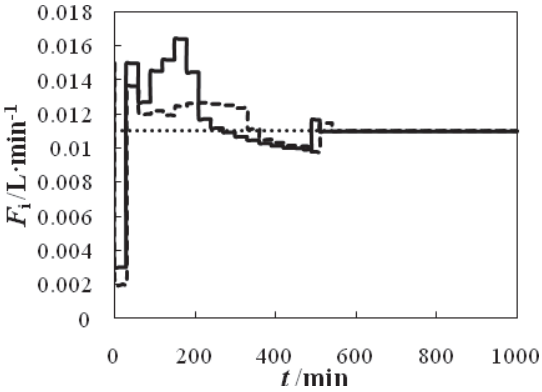

Fig. 2 Trajectory of F_i
— S_1; ---- S_2; ····· S_3

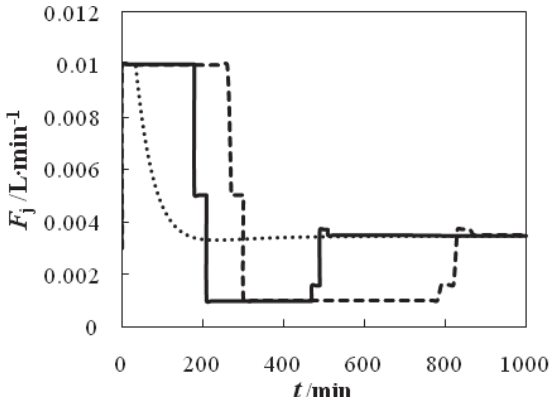

Fig. 3 Trajectory of F_j
— S_1; □□ S_2; ····· S_3

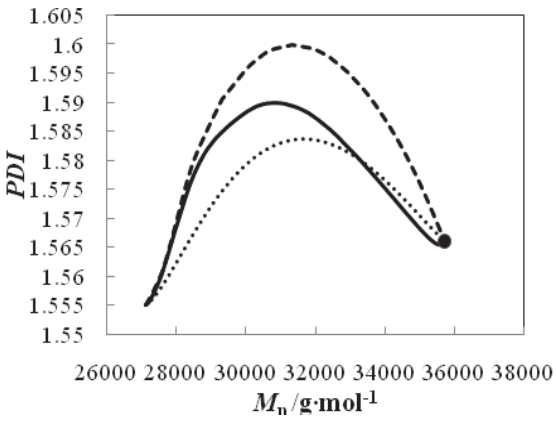

Fig. 4 Transition trajectory of M_n and *PDI*
— S_1; ---- S_2; ····· S_3; ● Target MWD

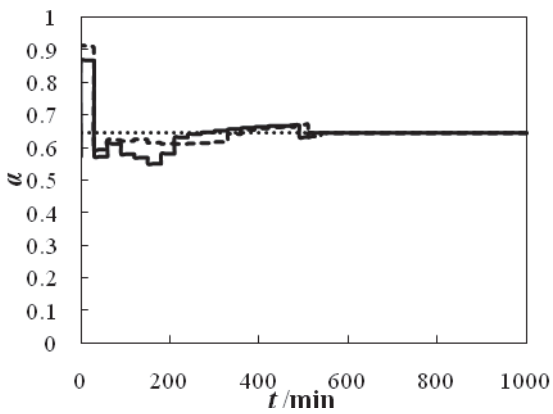

Fig. 5 Trajectory of α
— S_1; ---- S_2; ····· S_3

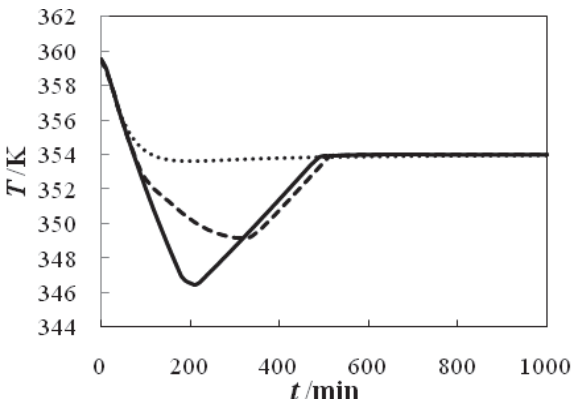

Fig. 6 Trajectory of T
— S_1; ---- S_2; ····· S_3

Table 4 Simulation results

Control systems	Transition time /min	Initiator consumption /L
S_1	717	8.23
S_2	730	8.11
S_3	1000	11.01

System S_1: Minimization J_1 + two regulatory controllers

System S_2: Minimization J_2 + two regulatory controllers

System S_3: Only two regulatory controllers (PID controllers)

6. Conclusion

The grade transition problem for free radical styrene polymerization in a pilot-plant CSTR is considered in this work. The polymer grade specification is defined as number average molecular weight M_n and polydispersity index *PDI*. The flow rate of initiator and coolant, F_i and F_j, are selected as manipulated variables in the dynamic optimization.

Dynamic optimization is required for shortening the operation time or minimizing the raw material consumption during the polymer grade transition in the CSTR. The optimal transition trajectories of manipulated variables were determined by off-line dynamic optimization. Simulation studies were carried out to verify the effectiveness of such control systems S_1 and S_2. System S_1 focuses on the transition time and system S_2 focuses on the amount of initiator consumption. The transition time of system S_1 was minimum and the amount of initiator consumption of system S_2 was minimum. Both systems satisfy the polymer grade specification at the end of the transition operation and are superior to the non-optimized naïve PID control system. This implies that the combination of the dynamic optimization and regulatory control system is necessary for optimal polymer grade transition operations.

References

[1] N. Padhiyar, S. Bhartiya and R. D Gudi. Optimal Grade Transition in Polymerization Reactors: a Comparative Case Study, *Industrial & Engineering Chemistry Research*, Vol. 45, No. 10, pp. 3583-3592, 2006.

[2] J. V. Kadam, W. Marquardt, B. Srinivasan and D. Bonvin. Optimal Grade Transition in Industrial Polymerization Process via NCO Tracking, *AICHE Journal*, Vol. 53, No. 3, pp. 627-639, 2007.

[3] M. H. Lee, C. Han and K. S. Chang. Dynamic Optimization of a Continuous Polymer Reactor Using a Modified Differential Evolution Algorithm, *Industrial & Engineering Chemistry Research*, Vol. 38, No. 12, pp. 4825-4831, 1999.

[4] G. Y Wei, J. D Wang and Y. R Yang. Optimal Grade Transition Based on Residence Time Distribution of Catalyst Particles in Bimodal Polyethylene Production Process, *Journal of the Chemical Industry and Engineering Society of China*, Vol. 60, No. 11, pp. 2847-2853, 2009.

[5] Y. Wang, H. Seki, S. Ohyama, K. Akamatsu, M. Ogawa and M. Ohshima. Optimal Grade Transition Control for Polymerization Reactors, *Computer & Chemical Engineering*, Vol. 24, pp. 1555-1561, 2000.

[6] S. BenAmor, F. J. Doyle Ⅲ and R. McFarlane. Polymer Grade Transition Control Using Advanced Real-Time Optimization Software, *Journal of Process Control*, Vol. 14, No. 4, pp. 349-364, 2004.

[7] C. Chatzidoukas, J. D. Perkins, E. N. Pistikopoulos and C. Kiparissides. Optimal Grade Transition and Selection of Closed-Loop Controllers In a Gas-Phase olefin Polymerization Fluidized Bed Reactor, *Chemical Engineering Science*, Vol. 58, No.16, pp. 3643-3658, 2003.

[8] H. S. Yi, J. H. Kim, C. Han, J. Lee and S. S. Na. Plantwide Optimal Grade Transition for an Industrial High-Density Polyethylene Plant, *Industrial & Engineering Chemistry Research*, Vol. 42, No. 1, pp. 91-98, 2003.

[9] M. Asteasuain, A. Bandoni, C. Sarmoria and A. Brandolin. Simultaneous Process and Control System Design for Grade Transition in Styrene Polymerization, *Chemical Engineering Science*, Vol. 61, No. 10, pp. 3362-3378, 2006.

[10] H. Y Lee, T. H Yang, I. L Chien and H. P Huang. Grade Transition Using Dynamic Neural Networks for an Industrial High-Pressure Ethylene-Vinyl Acetate (Eva) Copolymerization Process, *Computer &*

Chemical Engineering, Vol. 33, No. 8, pp. 1371-1378, 2009.

[11] A. Prata, J. Oldenburg, K. Andreas and W. Marquardt. Integrated Scheduling and Dynamic Optimization of Grade Transitions for a Continuous Polymerization Reactor, *Computer & Chemical Engineering*, Vol. 32, No. 3, pp. 463-476, 2008.

[12] Q. Guo, M. Noda and H. Nishitani. Optimization of Operating Conditions for Polymer Quality Control in a Continuous Stirred Tank Reactor, *Journal of Chemical Engineering of Japan*, Vol. 41, No. 5, pp. 394-402, 2008.

[13] Q. Guo, M. Noda and H. Nishitani. Determining Operating Conditions for Continuous Free Radical Polymerization with Specified Values of Molecular Weight Distribution Parameters, *Journal of Chemical Engineering of Japan*, Vol. 43, No. 11, pp. 956-959, 2010.

[14] M. P Stevens. *Polymer Chemistry - An Introduction*, 3rd ed., Oxford University Press, 1999.

[15] J. R Richards and J. P Congalidis. Measurement and Control of Polymerization Reactors, *Computer & Chemical Engineering,* Vol. 30, pp. 1447-1463, 2006.

[16] Process Systems Enterprise Limited (http://www.psenterprise.com/).

[17] S. M Ahn, M. J Park and H. K Rhee. Extended Kalman Filter-Based Nonlinear Model Predictive Control for a Continuous Mma Polymerization Reactor, *Industrial & Engineering Chemistry Research*, Vol. 38, No. 10, pp. 3942-3949, 1999.

[18] K. Y Yoo, B. G Jeong and H. K Rhee. Molecular Weight Distribution Control in a Batch Polymerization Reactor Using the On-Line Two-Step Method, *Industrial & Engineering Chemistry Research*, Vol. 38, No.12, pp. 4805-4814, 1999.

Copyright © 2012 DET Corp., Japan All Rights Reserved
International Journal of Comprehensive Engineering
Part B, 3(1), 25-31, 2014
Doi: 10.14270/IJCE2014.3.1.b25
Regular paper

ISSN 2186-2680
e-ISSN 2186-2656
www.iace-journal.org

Research on Portable Acoustic Emission Detection System Based on the Windows Program Design

Xianwei Wang [1], Guanghui Luo [1], Huaqing Wang [2], Sheng Bai [2] and Yuxin He [2, #]

[1] Equipment Management Department of Daqing Petrochemical Company, Daqing, 163000, China
[2] Chemical Safety Engineering Research Center of the Ministry of Education, Beijing University of Chemical Technology, Beijing, 100029, China

[#] Corresponding author: heyx0731@sina.com

Abstract: This paper states the principles of pipeline leak detection, the module structure and characteristics of USB AE, meanwhile, analyzes the limitations of the existing USB acoustic emission detection system. Based on the above, with Visual Studio 2012 as application development platform, windows 32 application project is designed and researched a portable USB acoustic emission detection system for pipeline leak. Furthermore, by pipeline leakage simulation experiments, we verify the system design is feasible, achieve the acoustic emission signal acquisition and data processing, and conducts noise analysis combined with the experimental data.

Keywords: Acoustic Emission, USB AE, System Development, Pipeline Leak Detection.

Received: May 25, 2012 / Accepted: Oct. 8, 2013 / Published: Jan. 6, 2014

1. Introduction

Pipelines are the arteries of petrochemical enterprise, it is self-evident that the importance of leak detection. Since the diversity of scene environment, the demand for flexibility of testing equipment is increasing. The portable acoustic emission testing equipment based on USB AE module, is a new type of acoustic emission devices possesses great flexibility than before, and it is also an important development of acoustic emission testing technology. Finally, it is significant for the promotion and application of acoustic emission testing technology.

Acoustic emission testing technology is a kind of passive detection technology, which determines the acoustic emission source information contained in these signals through “hearing” the acoustic emission signals emitted from the detected objects. In the process of acoustic emission testing, the internal pressure results that the pipeline medium inject to evoke transient elastic waves, and propagate from the pipe wall material to the surface, create the surface micro-displacement when the pipeline leaks out. If we place acoustic emission sensors on the pipe wall, it can translate micro-mechanical vibrations on the surface of the material to electrical signals by using piezoelectric effect, then the electrical signals are magnified, displayed and processed. In fact, acoustic emission signal is composed of one or some electrical signals processed by the system[1]. These signals which come from the leak points contained the characteristic information of source, and parsing these information can master the condition of leak pipe to achieve the purpose of leak detection.

This paper will elaborate the using of the USB AE module to design the portable multi-channel AE devices, and it is closely around how to improve the operability of the AE software system. This paper’s emphasis is the pipeline leak detection system based on the USB AE module[2]

2. The Hardware Structure

2.1 USB AE module

The module we used in this study is the high-performance USB AE module of American Physical Acoustics. Compared with the traditional AE boards, USB AE module is based on the USB (Universal Serial BUS) universal serial bus technology which makes the AE devices get ride of the PCI slots bound. Thereby, we can get rid of the bulky labor controlling machine. USB AE module can achieve the functions of real-time feature extraction and waveform acquisition and other functions.

USB AE module consists of 18-bit A / D converter, 20 M / s sampling rate and bandwidth of 1MHz, which integrates preamplifier circuit. The input and output signals of the amplifying circuit are analog signals which is an analog circuit with the magnification of 40dB, the pass band of 20KHz~1000KHz and the input noise voltage less than 5μv.

2.2 Multi-channel Portable USB AE System Hardware Design

The paper is designed to use multiple USB AE modules in order to build multi-channel AE system. By the use of RJ45 port, a four-channel system can be connected by four USB AE modules which can be shown in Figure 1.

This system is equipped with the R3a sensor of American Physical Acoustics Corporation Alpha series sensors, which has a peak frequency of 30kHz. The main function is to achieve the energy conversion between the mechanical energy and the electrical energy principle by using the Piezoelectric Effect. The 75Ω coaxial cable is selected to be the system signal cable.

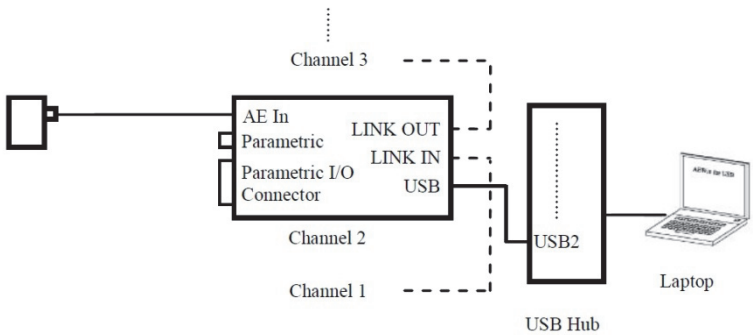

Fig. 1 USB AE hardware structure chart

3. The development of the software system

3.1 The limitations of the existing acoustic emission software system

C Most existing acoustic emission detection system are foreign system, which not suitable for domestic testing environment, and the operation settings are complex which needs a lot of experience, and the operational and applicability of the system are still need to be improved. For example, the setting of acoustic emission channel, which needs to set the threshold value, top and bottom limitation on analog flitter, sample frequency, pretrigger, length of each channel. Setting acoustic emission timing parameters PDT/HDT/HLT needs to take the detection of objects of different material in to account.

There are many acoustic emission parameters, such as the impact, event counts, amplitude, ASL value, RMS value, etc. But not all these parameters for different object detection is meaningful. It is easy for operators to be confused and can cause operation error. So we need to design portable USB acoustic emission detection system for a specific environment and object to meet the use requirements.

3.2 system development

3.2.1 Development Platform

In order to ensure software reliability and portability, the system software uses the Windows 7 operating system and Visual Studio C++ 2012 as a program development platform. Its high-quality code, readability, security and other advantages owe to the reliability, flexibility, high inheritance, easy to transplant and other characteristics of C++ language. C++ is the language which is very suitable for this study. The object-oriented feature of C++ ensures for the interface of the software and the realization of human-computer interaction.

VS2012 development platform is used to establish the win32 application project to develop software. Software interface is mainly divided into the menu bar, the main interface and the status bar. Main display needs to display waveform data, which can establish new pages and maps according to the needs. After

initializing global character, initializing the application and the main message loop, register the main window class.

After the registration, create window function is used to create the main window, and setting the window size, location, display style by setting the parameters in the function:

hWnd = CreateWindow(szWindowClass, szTitle, WS_OVERLAPPEDWINDOW, int *x*, int *y* , int nWidth，int nHeight, NULL, NULL, hInstance, NULL);

The hWnd is the handle of the window; szWindowClass is the type to create; the article is window class; SzTitleis the window title; WS_OVERLAPPEDWINDOW parameters makes the created windows of all styles, including title, system menu, border, minimize, maximize button and so on.

The message processing function of the main window is completed by LRESULT CALLBACK WndProc (HWND HWND, UINT message, WPARAM WPARAM, LPARAM LPARAM) function, whose main subject is switch structure. The judgment condition of switch is system message, the judgment situation of the case are mainly WM_CREATE, WM_COMMAND. The WM_COMMAND is generated by the window control, when you click on a control, the system will generate the message, so analysis menu options is done by identifying the message.

Menu option contains all the functions of software commands, which is the framework of software. Menu analysis program should be simple and clear. Lots of statements can't be written on the menu function ,which should be finished by calling the function and should be defined clear as far as possible. In the program of menu, every click will result in the connected of the certain ID, which can call the function to complete the order.

3.2.2 Acquisition module

The development of the system is based on the bottom of the development environment of American Physical Acoustics Corporation (PAC). The bottom of the development environment provides Dynamic Link Library to the development of the system, which is a mechanism of run-time application linked with library. By calling and accessing to the Dynamic Link Library, the system can control, manipulate USB card. Based on it, acquisition module completes the data collection activities by calling and analyzing the Dynamic Link Library provided by PAC company.

3.2.3 Acquisition module

This system makes full use of the bandwidth of USB bus. The design is multi-thread, while acquisition, storage and display are the independent thread. Each thread maintains a high degree of synchronization, so as to ensure the real-time performance of the system. The C++ system, which based on object oriented function, can achieve a human-computer interaction interface. In addition, data can also be displayed and analyzed.

In order to achieve functions of the reliability and accuracy of the system data transmission. A perfect function of data transmission protocol is designed. USB provides four transmission modes to ensure real-time connections among devices of the system. The transfer mode of the USB control is relied on to send a request to USB device to finish configurations, when USB AE device accesses computer to achieve configurations. While collecting data, the synchronous transfer mode of USB can guarantee the synchronous transmission of data. In other to ensure the accuracy of data transmission, the packet format is defined as the packet and head. Head stores version number, channel number, address and other information of data, and the encapsulation of head can improve the accuracy of packet transmission and sourcing. Head includes the type and information of data.

3.3 Pipeline leak detection module algorithm

3.3.1 Method for signal processing

Acoustic emission energy analysis method is suitable for continuous acoustic emission signals, and does not depend on any threshold voltage, so this paper adopts energy analysis method. Among the acoustic emission parameters, ASL value and RMS value reflect the size of acoustic emission, and cannot be influenced by threshold value. Meanwhile, they are extremely suitable for continuous acoustic emission, and they are easy to be measured, so ASL and RMS values are selected to judge pipeline leaks.

RMS voltage (RMS), which represents the root mean square of the signal in the sam-pling time, expressed as V. Average signal level (ASL), which represents the average signal level in the sampling time, expressed as Db.

Using energy analysis method for signal processing:

(1) Transform the 4-20*mA* current signal into voltage signal.

Acoustic emission sensor transforms the displacement which is generated by transient elastic waves which are gave out by the acoustic emission source into an electric signal, that is the 4-20*mA* current signal. The

system transform through signal processing to get 4-20mA current and 0-5V voltage value of the corresponding linear.

(2) RMS voltage (RMS):

$$RMS = \sqrt{\frac{1}{\Delta T}\int_{T_1}^{T_2}(V(t))^2 dt}\, Milivolt\,. \tag{1}$$

Where, $V(t)$ is a time-varying signal voltage value. $\triangle T$ is the average time, the value is T_2-T_1. Learned by the experiment that the value of $\triangle T$ is generally 0.5s-5s for leak detection.

(3) Average signal level (ASL):

$$ASL = 20\lg(RMS/1\mu V) - pre\,. \tag{2}$$

The system chooses the value of ASL as the decision value to evaluate whether the detected pipeline leaks or not qualitatively, which is also only major variable to estimate the leak rate of pipes and taps[3].

3.3.2 Location algorithm

The system is applied to the pipeline leak detection, positioning way are primarily for wire positioning and plane location. When the pipeline has large aspect ratio, we adopt the method of time difference wire positioning[i][4]; the planar positioning is used when the pipeline has a small aspect ratio. The development of this system, the main object to the pipe which has large aspect ratio, so the wire localization algorithm is adopted:

As shown in Figure 2, the acoustic emission source is between sensor 1 and sensor 2. $t1$, $t2$ is respectively the moment of sensor 1 or sensor 2 receives a time signal from the acoustic emission.

D is the distance between two sensors which can calculate the distance between the acoustic emission source and sensor 1.

$$d = \frac{1}{2}(D - \Delta t V)\,. \tag{3}$$

In the equation (3), V is the speed of sound waves in pipes, Δt is the time lag between two sensors received the signal.

As shown in equation (3), we only need to get the time lag Δt between two sensors received the signal, and the propagation velocity of sound waves in the test material, then the position of the leakage source can be calculated. The acoustic emission signal of pipeline leakage is continuous acoustic emission signal, the time delay between two continuous signal wave is obtained by cross-correlation method. The cross-correlation functions of two waves:

$$XY(\tau) = \frac{1}{\Delta T}\int_0^{\Delta T} X(t)Y(t+\tau)dt\,. \tag{4}$$

In the in equation (4), X (t) is the wave of a sensor X received from continuous source AE; Y（t+τ）is the wave of a sensor Y received from the same source AE; τ represents the time delay of $X(t)$; $\Delta\tau$ is a finite time interval and is in milliseconds. Δt is the lag of X and Y, two sensors receiving the wave by the same source AE emitted, can be get by the maximum peak of the cross-correlation function $XY(\tau)$, Δt=τ.

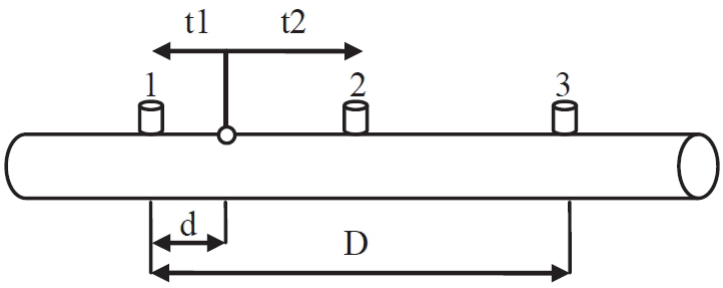

Fig. 2 Line positioning map of pipeline

4. Application experiment

4.1 Experimental facilities

We build a pipeline leak simulation platform, which uses a portable USB AE system to verify the validity and accuracy.

Laboratory table uses a seamless pipes with outer protective layer of long 2 m, diameter 100mm, thickness 10mm to simulate leak, On both ends of the pipe, the pump and valve are connected for pressurizing and pressure regulator. In this experiment, the tube medium is water, when the experiment, by the head of 28m of decay energy pipeline pump pressurized to 0.3MPa. Pipe connected to the pump end is viewed as zero point, the AE sensor is set in the axial direction 0.7m, 1.3m respectively. The detection position of the outer protective layer of the tube is removed 7-8 square centimeters in order to security for acoustic emission sensor. For analog leak hole, in the axial direction, away from the zero position of 1.25m to play 1.2mm diameter holes, as in Figure 3. Another air pump will be run when experiments in order to simulate the field of environmental noise.

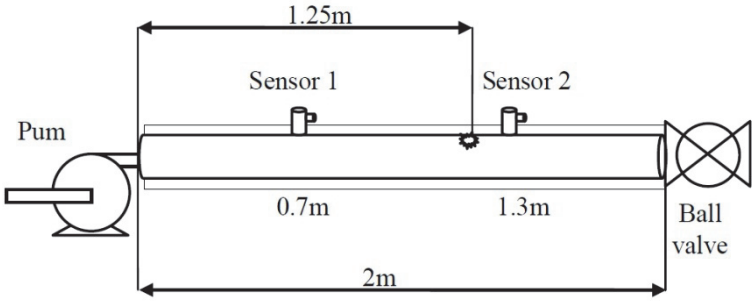

Fig. 3 Pipeline leak simulation platform

4.2 Experimental procedure

(1) The parameter settings. Closing the simulated leak hole and opening air pump of simulating environmental noise, applying software to measure noise in order to set the threshold values. After measurement, the noise signal is 26dB, and therefore the threshold value is set to 30dB. Blocking the leak hole, when the pipeline pressure to 0.3MPa stably, collecting is started, while ASL is 14dB, ASL alarm value is set to 30.

(2) Establish the diagram of ASL value variation over time, the diagram of the RMS value with time variation, the diagram of variation with time of impact and the diagram of power spectrum.

(3) Open leak hole, when the pipe pressure stabilized at 0.3MPa, begin to the acquisition and observation image, as Figure 4.

(4) Leak point positioning and calculation error, and error analysis. Sensor for the four different location positioning experiments in four groups. Sensor setting and the leakage point positioning data of the experiments are shown in Table 1.

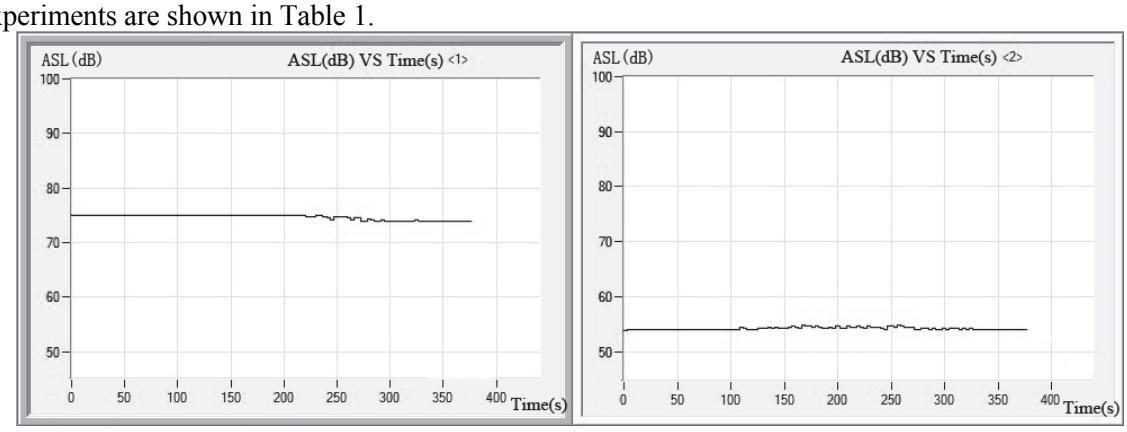

Fig. 4 AE Signal spectrum

4.3 Figures and Tables

(1) When the pressure is stable and collection is begun, ASL is stable and significantly higher than the alarm value. Description of the pipeline system can be effectively monitored for leaks.
(2) Four groups positioning experiments are integrated to verify the system can complete pipeline leak point positioning function, But the data as you can see, there is a error of positioning:

Table 1 four groups of experimental data leak point positioning

	Sensor1 coordinate(m)	Sensor2 coordinate(m)	Positioning data(m)	Real location (m)	Relative error
Group 1	0.7	1.3	1.19	1.25	4.8%
Group 2	0.7	1.5	1.16	1.25	7.2%
Group 3	0.9	1.3	1.21	1.25	3.2%
Group 4	0.5	1.5	1.14	1.25	8.8%

Positioning errors may result from: (1) inaccuracy of the system algorithms; (2) the environment impact on the positioning; (3) inaccuracy of the sensor; (4) the attenuation of the acoustic emission signal of the pipe material, etc.

From the above results it can be seen, the system can accurately determine the pipeline leakage, related data of the map can be established for analysis, leakage signal according to the location of the leak can be positioned. To sum up, we can prove that the system can achieve the expected functionality.

4.4 Noise Analysis

Acoustic emission techniques are susceptible to noise signals, so the noise signal of the filter is very important in the process of acoustic emission testing. Field testing environment in the tank will usually have a mechanical noise, electromagnetic noise and environmental noise.

Storage tanks will be connected to have different mechanical structures according to different purposes, such as manholes, ladder, insulation layer and a variety of instrumentation. As the wind, temperature changes, these mechanical structures produce mechanical noise by friction. During testing the bottom of the tank, the guard sensors should be arranged to filter the AE signal which comes from the upper of the sensor and does not belong to the tank bottom. Tank surrounding environment changes, such as wind, rain, high temperature and other acoustic emission testing will also have a relatively large impact.

Acoustic emission-line detection will inevitably encounter electromagnetic noise, some of which comes from the equipment itself[5-6], but also comes from the surrounding environment of electromagnetic interference. Different from mechanical noise, electromagnetic noise tends to produce continuous signal, and has more compact on acoustic emission testing. For electromagnetic interference signal with specific frequency spectrum characteristics, the preceding filtering method is adopted to wipe out the interference of electromagnetic noise.

5. Conclusions

With the powerful C++ program language, we design and develop the portable USB acoustic emission for detecting the leak of the conduit. The system is proved to be feasible through the pipeline leakage simulation experiment and it also has the function of acoustic emission of real-time data acquisition, storage, display and determining the location of the sound source. Compared with the traditional general acoustic emission system, this system in pipeline leakage detection shows excellent performance, simple interface, convenient operation, good applicability, and has wide application prospect.

At present, the specific object of portable USB acoustic emission system has just started. It is still insufficient in pipeline leakage estimation and positioning accuracy of the amount, which needs to be studied further.

The focus of future research is as follows:
(1) The algorithm should be studied further and system needs to be developed for other detection objects.
(2) Focuses on different defect characteristics of acoustic emission signal analysis, design flaw identification module.

References

[1] *Terminology for Nondestructive Examination*, ASTM E1316−1996.

[2] J. Sell. Overview of New Acoustic Emission (AT) Systems, *EWGAE*, pp. 691-698, 2004.

[3] W. Kaewwaewnoi, A. Prateepasen and A. Kaewtrakulpong. Investigation of the Relationship Between Internal Fluid Leakage Through a Valve and the Acoustic Emission Generated from the Leakage, *Measurement*, Vol. 4, pp. 274-282, 2010.

[4] R. K. Miller, A. A. Pollock, D. J. Wats, etc. A Reference Standard for the Development of Acoustic Emission Pipeline Leak Detection Techniques, *NDT&E*, Vol. 32, No. 1, pp. 1-8, 1999.

[5] L. N. Stepanova, K. V. Kanifadin, I. S. Ramazanov. The Influence of Temperature on the Characteristics of Piezoelectric Transducers and Errors of Localization of Acoustic Emission Signals, *Russian Journal of Nondestructive Testing*, Vol. 46, No. 5, 2010.

[6] C. Auerswald, A. Sorger, M. Dienel, A. Shaporin, J. Mehner. MEMS Acoustic Emission Sensor with Mechanical Noise Rejection. Systems, Signals and Devices (SSD), *2012 9th International Multi-Conference*.

Copyright © 2012 DET Corp., Japan All Rights Reserved
International Journal of Comprehensive Engineering
Part C, 3(1), 32-37, 2014
Doi: 10.14270/IJCE2014.3.1.c32
Regular paper

ISSN 2186-2680
e-ISSN 2186-2656
www.iace-journal.org

The Shock Response Spectrum of two degree-of-freedom-system under the Action of TerminalPeak Sawtooth Pulse

Jiuhong Jiang [1,#], JinZhi Zhou [1]

[1]Department of Mechanic Engineering, Hubei University of Technology, Wuhan, 430064, China

[#]Corresponding author: wdm8518@126.com; Tel.: +0086-13871362132

Abstract: The cushioning packaged system is always predigested as a two-degree-of-freedom system. In order to study the effect of nominal frequency ratio, damping ratio, mass ratio and the amplitude of the terminal peak saw tooth pulse on the shock response spectrum of the critical element and the main part reaction of cushioning packaging system material, a method based on fourth order Runge-Kutta algorithm is proposed in this paper. The experimental results show that the proposed method has an important application in the design of cushioning packaging.

Keywords: Terminal Peak Saw Tooth Pulse, Shock Response Spectrum, Damping Ratio, Nominal Frequency Ratio.

Received: May18, 2012/ Accepted: Aug. 12, 2013 / Published: Jan. 6, 2014

1. Introduction

Shock response spectrum is an important base to evaluate the reliability of cushioning packaging system. The main causes for damage of package system are vibration and shock during transportation, and the critical element always be damaged at the first, so it is more precision to predigest the packaged products as an two-degree-of-freedom system[1]. Wang Z-W [2,3] has studied shock response spectrum and damage boundary curve of single degree-of-freedom system under different pulsed excitation, Z.W. Wang and J. Wang [4,6] has proposed the concept of three-dimensional shock spectrum and damage boundary surface with tangent system. Considering that the terminal peak saw tooth pulse is the most common, this paper will investigate the shock response spectrum of both main body and critical element of two-degree-of-freedom system under the action of terminal peak saw tooth pulse, and discuss the effect of nominal frequency ratio, damping ratio as well as mass ratio.

2. Dynamic equations and non-dimensional equations

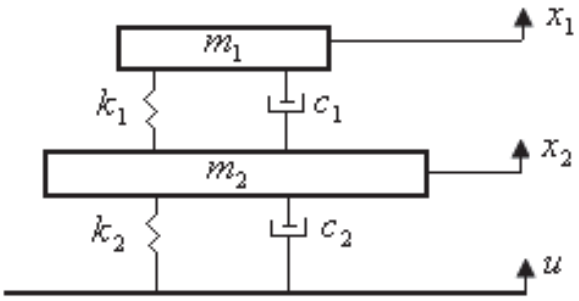

Fig.1 Dynamic model of packaging system with critical element

The dynamic model of packaging system with a critical element is shown in Fig. 1, where $m_1$and $m_2$are the mass of critical element and main part respectively, $k_1$and c_1 are the equivalent linear elasticity coefficient and equivalent damping ratio of the two parts, $k_2$and c_2 are the linear elastic coefficient and damping ratio of cushioning material respectively. This paper studied dynamics response characteristics of the system under the terminal peak saw tooth-pulse, the function is $\ddot{u} = u''_{0m} \frac{t}{t_0} \Delta H(t, t_0)$.

The differential equations of two degree-of-freedom system under terminal peak saw tooth pulse can be written as:

$$\begin{cases} m_1 \ddot{x}_1 = k_1(x_2 - x_1) + c_1(\dot{x}_2 - \dot{x}_1) \\ m_2 \ddot{x}_2 = k_2(u - x_2) + c_2(\dot{u} - \dot{x}_2) + k_1(x_1 - x_2) + c_1(\dot{x}_1 - \dot{x}_2) \end{cases} \tag{1}$$

Non-dimensional displacement and time were introduced:

$X = \frac{x-u}{L}, U = \frac{u}{L}, \tau = \frac{t}{T}, T = \sqrt{\frac{m_2}{k_2}}$. And define: $\zeta_1 = \frac{c_1}{2\sqrt{m_1 k_1}}$, $\zeta_2 = \frac{c_2}{2\sqrt{m_2 k_2}}$, $\alpha = \frac{m_1}{m_2}$, $\lambda = \frac{\omega_1}{\omega_2}, \omega_1 = \sqrt{\frac{k_1}{m_1}}, \omega_2 = \sqrt{\frac{k_2}{m_2}}$, where X' and X'' are first derivative and second derivative respectively. Applied a terminal peak saw tooth acceleration pulse excitation on the base, and the non-dimensional equation is:

$$\begin{cases} X_1'' = \lambda^2(X_2 - X_1) + 2\lambda\zeta_1(X_2' - X_1') - U'' \\ X_2'' = -X_2 + \lambda^2\alpha(X_1 - X_2) + 2\zeta_1\lambda\alpha(X_1' - X_2') - 2\zeta_2 X_2' - U'' \end{cases} \tag{2}$$

$U'' = U''_{0m}\Delta H(\tau, \tau_0)$, Where U''_{0m} is the amplitude and τ_0 is the width of the terminal peak saw tooth acceleration pulse.

$$\ddot{U} = \begin{cases} U''_{om} \frac{\tau}{\tau_0} (0 \le \tau \le \tau_0) \\ 0 \qquad (\tau \ge \tau_0) \end{cases} \tag{3}$$

According to Eq. 2 and Eq. 3, the factors that influence the maximumvalue of acceleration response are: mass ratio, nominal frequency ratio, damping ratio of the main body and critical element as well as impact time τ_0.

3. Shock response spectrum of main part and critical element

In order to evaluate the damage of the product during transportation, the maximum shock response spectrum is usually chosen to describe the response of the product on the impulse. Eq. 1 and Eq. 2 generally discussed shock response spectrum of two-degree-of-freedom system, thus the fourth order Runge-Kutta method is applied. The mass ratio is much smaller than 1 due to the simplification of packaging system, here the mass ratios are $\alpha = 0.001, 0.01, 0.1, 0.8$, frequency ratios are $\lambda = 0.01, 0.1, 1, 5$ and damping ratios are $\zeta_1 = 0,\ 0.01,\ 0.1,\ 0.5$ and $\zeta_2 = 0,\ 0.01,\ 0.1,\ 0.5$ respectively.

Since the shock response spectrum of two -degree-of-freedom system is a three-dimensional surface, the projection to the planes $2\pi f_0 t_0 - \ddot{x}_{1m} / \ddot{u}_m$ and $2\pi f_0 t_0 - \ddot{x}_{2m} / \ddot{u}_m$ to investigate the effect of each parameter clearly, where $r = f_{n2} / f_0$, $\beta = \ddot{x}_m / \ddot{u}_{0m}$.

4. Discussion of the results

Fig. 2(a-d) indicates the effect of frequency ratio on the shock response spectrum. It is found that frequency ratio has great impact on shock response spectrum of the critical element, and the response is biggest when the frequency ratio is approximate 5, moreover, the response is also influenced by mass ratio, the amplitude of the response spectrum decrease as the mass ratio increasing(except $\lambda=1$). But frequency ratio and mass ratio have little effect to the shock response spectrum of main body, it is almost the same as the single degree-of-freedom linear system, which decreases gradually after peak value and finally tends to 1.3. β

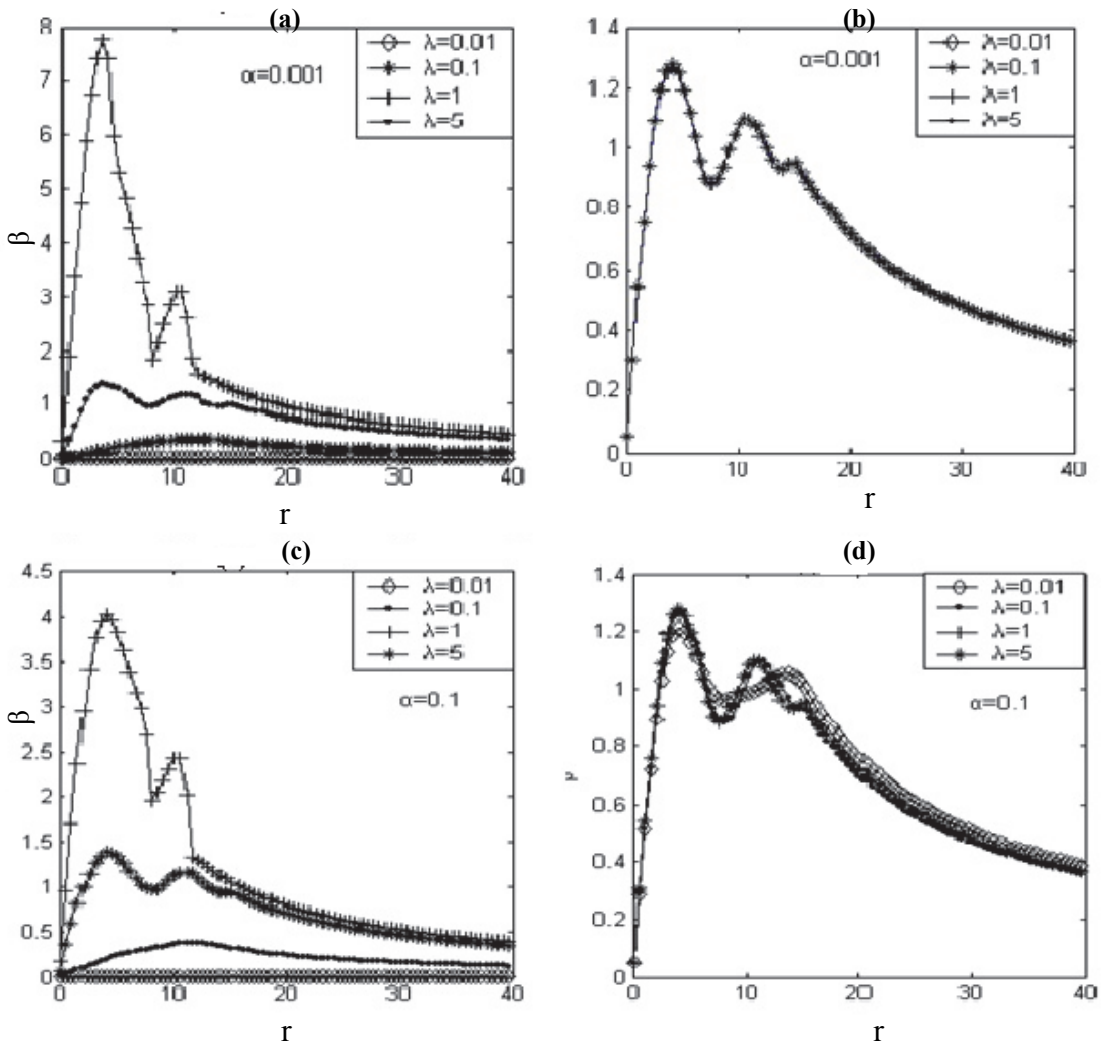

Fig. 2 SRS for packaging system with different frequency ratio (ζ1=0, ζ2=0)
(a) SRS of critical element. (b) SRS of the main part. (c) SRS of critical element. (d) SRS of the main part.

Fig. 3(a-f) shows the effect of mass ratio on the shock spectrum. It is shown that mass ratio has little influence on the shock response spectrum of main body and critical element mainly because the mass of critical element is much smaller than main body, thus the impact of critical element to the main body could be neglected while frequency ratio is much smaller than 2; while frequency ratio is much bigger than 2, response spectrums of main body and critical element are almost the same, the response spectrums move upward as mass ratio increasing, while frequency ratio is approximate to 2, the response of critical element increases as mass ratio decreasing, and it has very little influence on main body. When $\lambda=1$, the response spectrum of the critical element is much bigger than the other cases, so this case should be avoided in the packaging design.

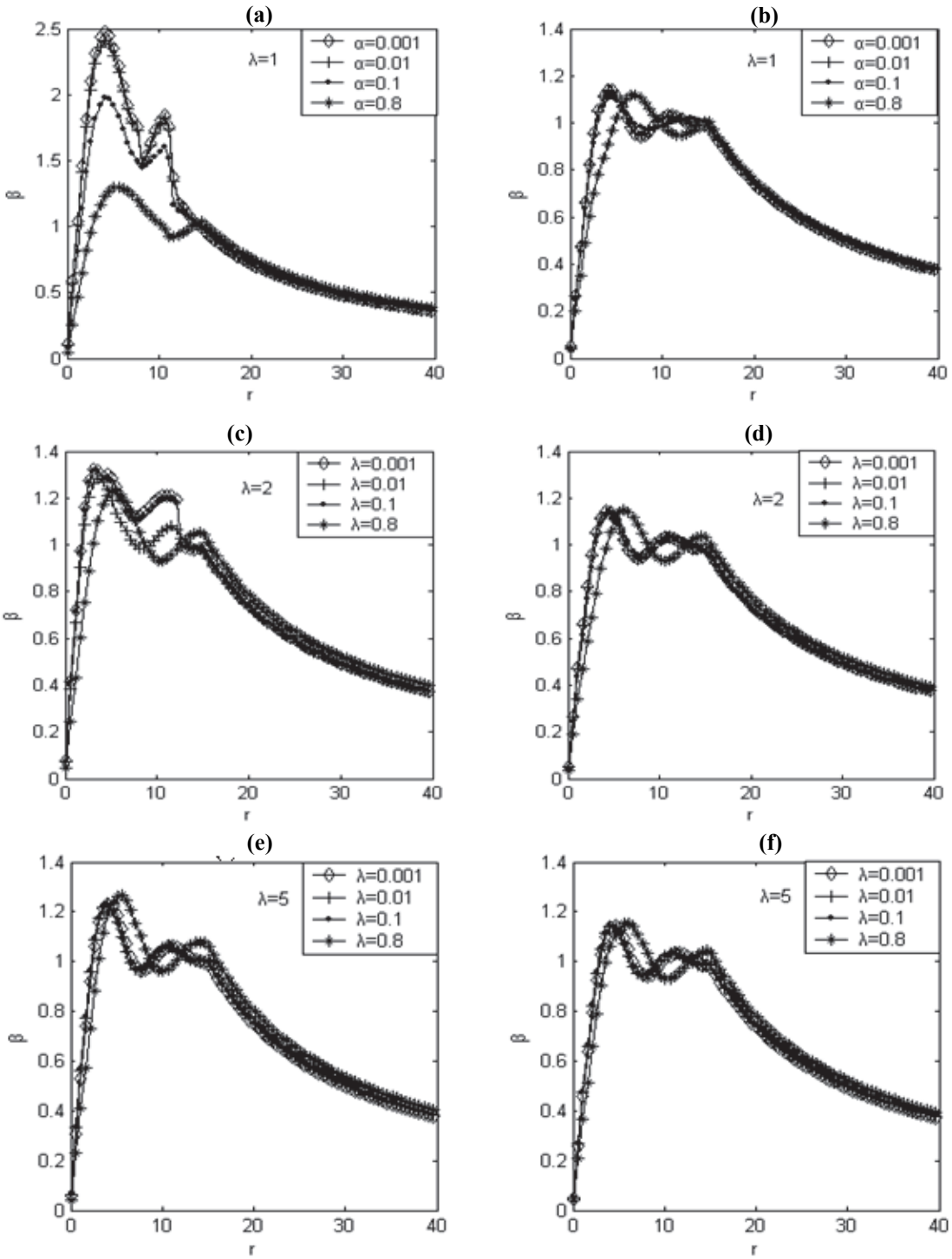

Fig. 3 SRS for packaging system with different mass ratio (ζ_1=0.1, ζ_2=0.1)

(a) SRS of critical element. (b) SRS of the main part. (c) SRS of critical element. (d) SRS of the main part. (e)SRS of critical element. (f) SRS of the main part.

Fig. 4(a-d) shows the effect of damping ratio on the shock spectrum. The critical element damping ratio that connecting the main body and critical element could effectively reduce shock response spectrum and has little influence on main body of the product, while the damping ratio of the main body (cushioning material) could sharply reduce the shock response of critical element. These two damping ratios have the same influence on critical element, the shock response of main body decreases as damping ratio increasing.

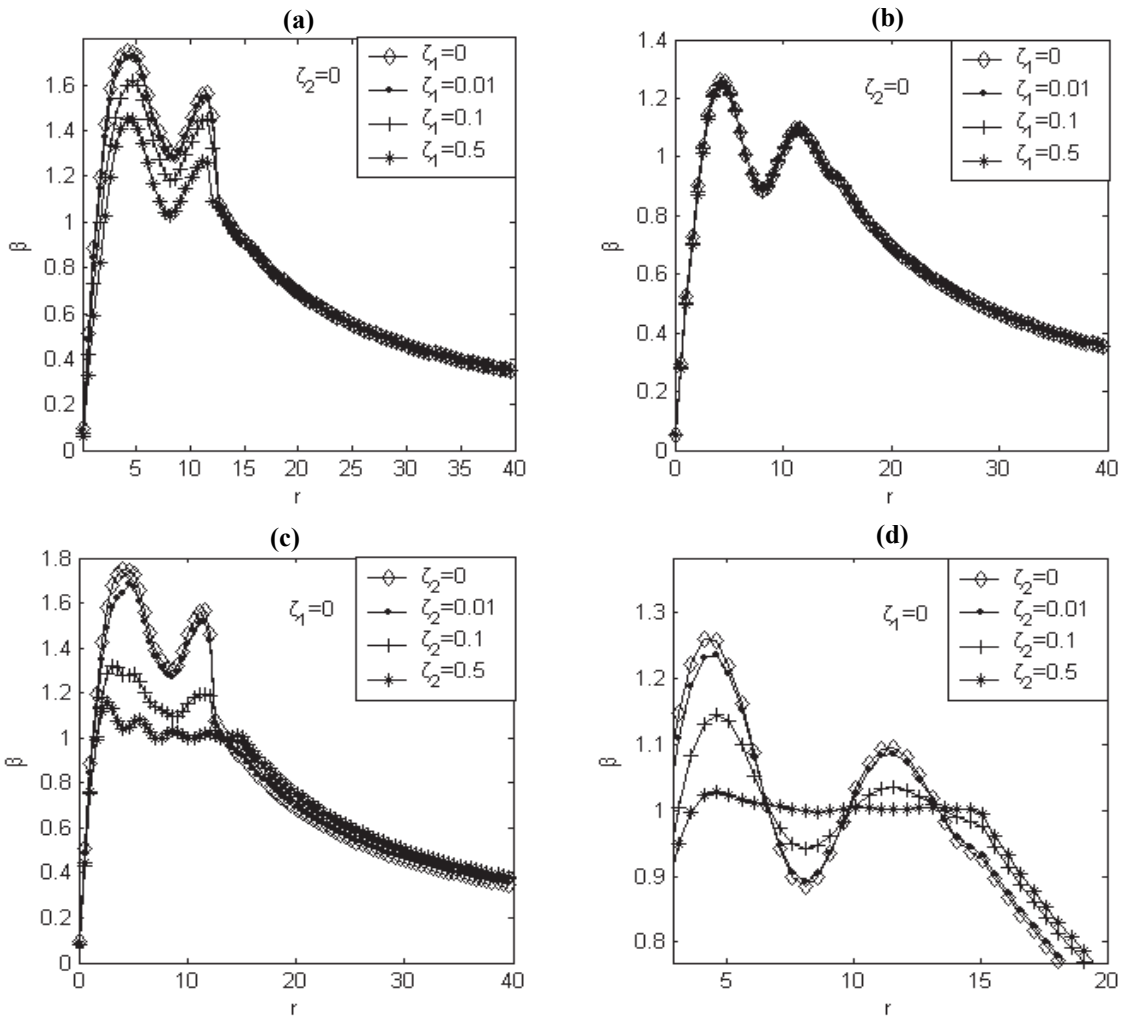

Fig. 4 SRS for packaging system with different damp ratio (α=0.1, λ=2)
(a) SRS of critical element. (b) SRS of the main part. (c) SRS of critical element. (d) SRS of the main part

5. Conclusion

a. The shock response spectrum of two degree-of-freedom system under terminal peak saw tooth pulse is directly related with mass ratio, nominal frequency ratio without coupling, damping ratio of main body and critical element;

b. The shock response spectrum does not rely on the peak value of shock wave, for the system is linear simplified, and the response spectrum is almost the same as that of single degree-of-freedom system because in the packaging system, mass ratio of main body to critical element is much smaller than 1, therefore, the impact could be neglected;

c. The response of critical element reaches the summit while non-coupling frequency ratio is around 5, so that it could be reduced by choosing cushioning materials to adjust the frequency ratio in cushioning package design;

d. Damping ration could effectively reduce the response amplitude, thus it can be fully used in the cushioning packaging design.

Acknowledgements

The authors would like to gratefully acknowledge this support by Research Project of Science and Technology of Hubei Province Education Department (D20111406) and Project of Research Funds for the Doctoral Program of Hubei University of Technology (BSQD0915).

References

[1] J.H Jiang and Z.W Wang, Analysisthe Effects of Fragility'S Response in Dropping Based on Matlab, *Journal of Packaging Engineer*,Vol.25, pp.33-34, 2004.

[2] Z. W Wang. Shock Spectra and Damage Boundary Curves for Hyperbolic Tangent Cushioning System and their Important Features, *Packaging technology and science*, Vol. 14, pp. 149-157, 2001.

[3] Z. W Wang.On Evaluation of Product Dropping Damage, *Packaging technology and science*, Vol. 15, No. 3, pp. 115-120, 2002.

[4] Z. W Wang and J. H Jiang. Evaluation of Product Dropping Damage Based on Key Component, *Packaging technology and science*, Vol. 23, No. 6, pp. 263-266, 2010.

[5]J. Wang and J. H Jiang. Dropping Damage Evaluation for a Tangent Nonlinear System with a Critical Component, *Journal of Computers and Mathematics with Application*, Vol. 8, pp. 263-267, 2010.

[6] J. H. Jiang and J. Z Zhou. The Shock Response Spectrum of Packaging System with a Key Component under the Action of Preceding Peak Saw Tooth Pulse, *2011 International Conference on Mechanical Engineering and Technology*, Vol. 13, pp. 427-431, 2011.

Copyright © 2012 DET Corp., Japan All Rights Reserved
International Journal of Comprehensive Engineering
Part C, 3(1), 38-42, 2014
Doi: 10.14270/IJCE2014.3.1.c38
Regular paper

ISSN 2186-2680
e-ISSN 2186-2656
www.iace-journal.org

Fixed Deck Foam Extinguishing System on the Sea

Feng Wang [1], Hongwu Chen [1,#], Can Wang [1], Shuai Zhang [1], Ting Gao [1]

[1] Engineering College, Shanghai Ocean University, Shanghai, 201306, China
[#] Corresponding author: hwchen@shou.edu.cn; Tel.: +86-21-61900817; Fax: +86-21-61900805

Abstract: With the development of global economy, marine transportation has been presenting busier scene, global coastal port, especially the throughput of China port continues to increase, all kinds of dangerous chemicals transports and the increased wharfs, which is because the geography particularity of waters, also added the ship fire control work new difficulties. For the particularity of large oil tankers and various inflammable and explosive chemicals transport ship, this article briefly introduced the sea foam fire extinguishing system. Firstly, the selection of proportion mixer is introduced, and then briefly introduces the principle and characteristics of fixed deck foam fire extinguishing devices.

Keywords: Large Oil Tanker, Proportion Mixer, Fixed Deck Foam Fire Extinguishing Devices.

Received: May 25, 2012 / Accepted: Aug. 12, 2013 / Published: Jan. 6, 2014

1. Introduction

Fire accident on the sea can be prevented, but it is hard to avoid. Once the trend of fire appears, we must control the fire quickly, and prevent its spread quickly, or it will cause more damage. Oil tankers, as energy transport sailing on the sea or in the process of carrying out, is easily caught fire accident. According to statistics, since 2002, there have been 28 more serious fire and explosion accidents of oil tanker worldwide, because no timely help on the sea, once improperly disposed, it is easy to get the ship destroyed seriously, and also can cause serious marine pollution accidents. Therefore, preventing oil tanker accident and control the fire, developing advanced foam fire system is of great significance.

Due to the particularity of large oil tankers and various inflammable and explosive chemical transportation ships, the carried most oil chemical products flash point is low, easily gasified, once caught fire, fire trend will be rapid, and forms an explosive fire, which is of great difficulty to extinguish [1]. The general fire water usually works not so well, while foam fire extinguishing presents its incomparable advantages. Foam fire extinguishing devices can spray bubble liquids which can quickly isolate the inflamed and explosive oil and air goods, protect the important instrument, and realize fast extinguishment. Fixed foam fire extinguishing system is important fire control facility of deck cargo ship, whether the system is available in immediate state, will directly relate to the ship security, and the proportion mixer is the core component [2]. Foam fire extinguishing system is mainly used on the oil tanker and amphibious ship. Conventions and standard requirements: tankers which load crude oil or oil products whose flash point (closed glass test) is no more than 60 □ and ray stream pressure is lower than the atmospheric pressure and oil tanks which carry the products and with the same fire dangerous liquid product goods, for 500 tons gross and above but less than 20000 tons of oil tanker loads, should be fixed with deck foam fire system [3].

The fire extinguishing system is made by bubble stoste and sea water, which are primarily mixed by proportion mixer with the proportion 3%-6%, then mixed intensively with pipeline, the mixed liquid is driven by a pump to the spout and spray out into sky with the air and form bumbles, the bumbles cover on the surface of the burning goods, isolate oxygen and cool the fire temperature and then extinguish the fire. Bubble stoste is made up with animal protein and water decomposition and filled with stabilizer and preservative, presenting black brown and flavor is strong. The bubble fire extinguishing devices can be classified into animal protein bubble fire extinguishing device and fluorine protein bubble fire extinguishing device. By bubbling times, it is classified into low power (12:1), medium (between 50:1 and 150:1) and high powers (more than 150:1) these three types [4].

2. Selection of Foam Proportion Mixer

Large oil tankers and all kinds of chemical goods transport ships are often sailing on the sea, work environment is bad, and often encounter strong wind surge, once appear fire accident, it will be always hard to get the land rescue for help. Therefore, the principle of selection of sea foam mixing ratio device should be taken into main consideration as listed below. First, it is stationary. Due to the limited space in the ship and all kinds of swing, it is inconvenient for mobile ship. Second, the storage capacity is enough for foam liquid, flow pressure range is wide, and mixture ratio is accurate. Third, it should be high reliability, convenient in use.

At home and abroad the bubble mixing ratio device is mainly divided into five: pipeline pump suction, ring suction, storage tank pressure type, pump into the balance pressure type, and spoon-feed [5]. The first two belong to negative pressure foam mixing ratio device, the third four or five for positive pressure type foam mixing ratio device. Pipeline pump suction and ring suction foam mixing ratio device are suitable for small flow and pressure, mainly used in mobile foam firefighting equipment, such as foam cart, foam fire engines, etc. And in fixed foam fire-extinguishing systems, the tank pressure type or pump into the balance pressure type foam proportion mixing device are generally used [3].

For the above five kinds of foam mixing ratio device, pipeline pump suction and ring suction foam mixing ratio device , due to its small range of flow rate and pressure, and more restrictions when design the ring pump type foam proportion mixing device system, are difficult to design, some designers can not deal with the faced difficulty and cannot make the designed system work normally, this may be the reason why mixing ratio was left out, and it is main used in mobile foam fire extinguishing equipment, such as foam cart, foam fire truck, fireboat, etc. Spoon-feed bubble mixing ratio is the same small flow device that is currently used only in the low proportion of A kind of bubble of mixing fire extinguishing system. Therefore, these three kinds of foam mixing ratio device is not easy to choose in the large oil tankers and various inflammable and explosive chemicals transport ship.

Tank pressure type foam proportion mixing device and pump into the balance pressure type foam proportion mixing device are applicable for wide flow pressure range and accurate proportion of mixture [6], apply to fixed or half fixed type foam fire extinguishing system, and meet the conditions of sea foam proportion mixing device selection.

Tank pressure type foam mixing ratio device for its installation and use are simple and convenient, performance is stable, is widely produced and used in fire engineering areas, the technical research has been also thorough. At present the domestic production enterprises of fire extinguishing are as many as a dozen; the product's design theory, applied technology research literatures are a lot. For pump into the balance pressure type foam proportion mixing device its foam liquid storage capacity is bigger, reliability is higher, more flexible when compared to the tank pressure type foam proportion mixing device [7]. Foam cans that is used by tank pressure type foam proportion mixing device must be able to withstand the pressure of the fire water pressure tank, and put forward the relevant national standards for the diaphragm type pressure tank, considering the influence of use caused by the diaphragm materials performance, its volume should not be greater than 5000 L. For without the diaphragm of the integral or space type foam cans, considering rest after will all or part of the waste after liquid foam is one time used up, and considering the manufacturing costs, its volume also should not be too big, commonly 13000 L. The following for pump into the balance pressure type foam mixing ratio device, its bubble of the tank is the general can, also can use any form of foam liquid storage vessel or storage tank and its capacity can reach 25000L or even greater. After one time use, residual liquid foam still can continue being used; bubble fluid can also be added in use at any time. In addition, adopt the automatic pressure regulating for liquid equipment, it can also be equipped with more identical or different specifications of foam proportion of mixer compound pump into the balance pressure type mixing ratio device, for multiple pipeline system being provided with bubble mix and fluid. Therefore, pump into the balance pressure type ratio mixing device is especially suitable for large-scale petrochemical industry transports, oil tank area, petrochemical dock, hangar, and other important fire danger occasion.

3. Current Forms

Commonly used types are chemical foam and the air bubble, air foam fire extinguishing system is widely used in the ship. And air foam system is divided into low multiples foam fire system and high multiples foam fire extinguishing system, namely the positive pressure type foam fire extinguishing system and negative pressure type foam fire extinguishing system. Low multiple bubbles are composed by the foam space (foam ark), proportional valve, and fire pump constitute [8].

Three different ways are divided according to the mixture differences between seawater and stock bubbles:

(1) Pressure type of hybrid method

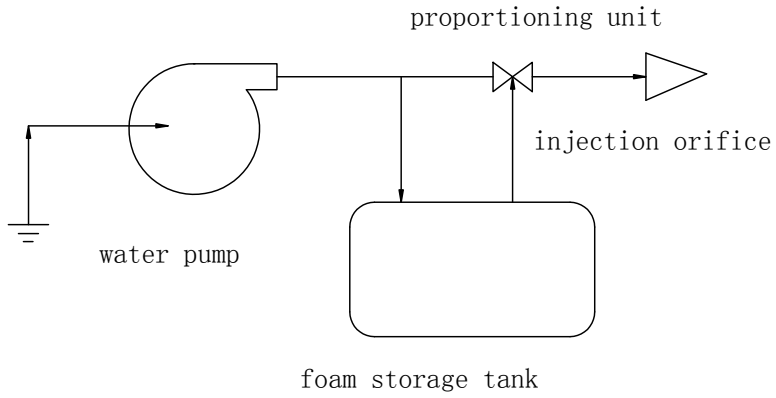

Fig. 1 Pressure typed hybrid method

Part of the sea water is pumped into the storage tank or the storage locker by fire pump, and to keep the certain internal pressure, at the same time, most of the sea water through the proportion is mixed by the injection machine and role will suck out stock mixture, then adjust the mix proportion, make the mixture liquid ejected into the air from bubble cannon (gun) mouth with high-speed and contact the air and then form the foam. The biggest drawback is that if use foam system, store the bubble of the ark directly with seawater does mix, it belongs to be disposable, therefore can not be daily function tested, so it is already washed out gradually.

(2) Suction pipe direct mix method

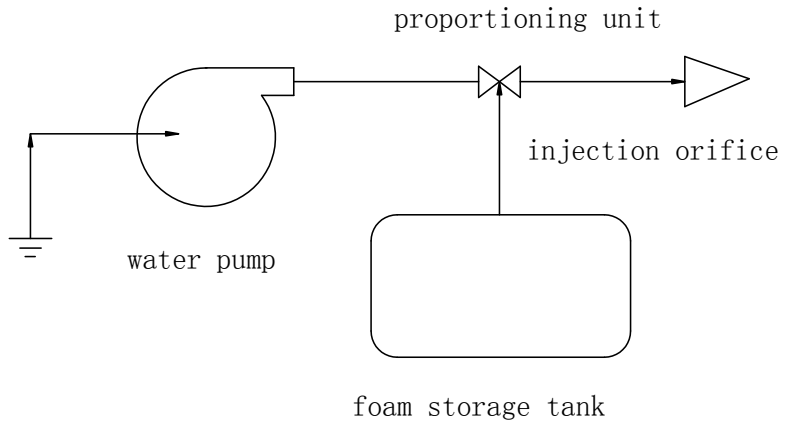

Fig. 2 Suction pipe direct mixing method

The working principle of vacuum typed foam fire system is, by the fire pump seawater directly input ratio of mixer inlet, shrinkage effect caused by mouth suck the entrance liquid foam vacuum, it is similar to the thrower suction action that will stock bubble from storage tank inhaled proportion mixer, mixed, directly through the pipe again from bubble gun nozzles injection.

(3) Suction pipe in circulation mix method

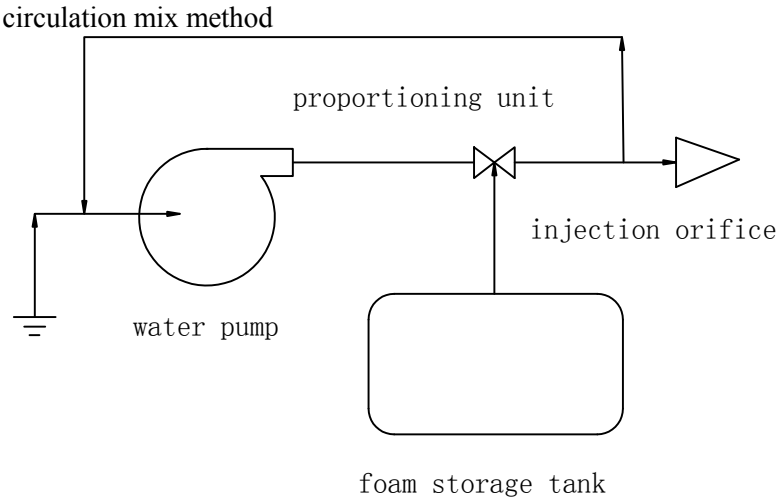

Fig. 3 Suction pipe in circulation mixing method

On the basis of the hybrid method, then make the liquid in the pipeline ejection mouth of proportion mixer to fire pump feed line, to recycle part of the mixture to achieve full mixing action, again by the introduction of the fire water ratio mixer pipe to foam injection nozzles gun [2] [8] [9] [10].

4. Discussion

The front analyzes the choose of proportion of foam mixer, by analyzing, pressure type foam proportion mixer and pump into the balance pressure type foam proportion mixer are suitable for sea foam fire extinguishing system, but common sea foam fire extinguishing system is relatively backward. Therefore, this paper takes advantages of tank pressure type mixer and pump into the balance pressure type mixer, design two new proportion of the mixer.

(1) Storage tank pressure type foam mixing ratio system

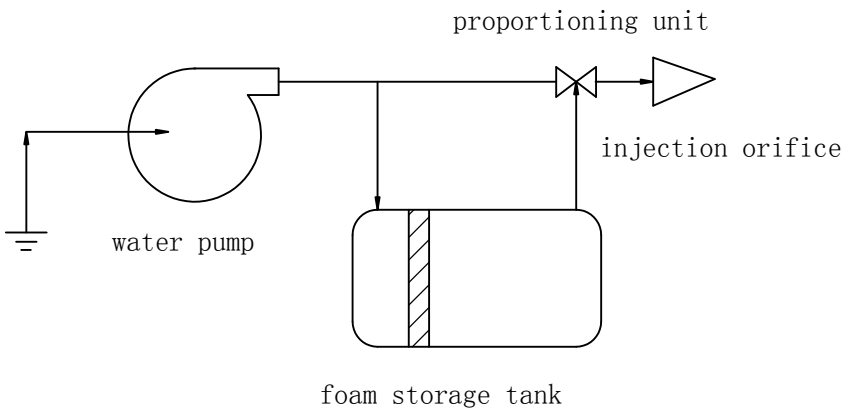

Fig. 4 Tank pressure typed mixing method

When the system startup, fire pump transports pressure flow of water through the main device of bubble mixing ratio, in the front of reduced pressure hole board, a small part of the high pressure water flow through the feed line into the pressure on the left side of the storage tanks, punch and replace the same volume of bubble liquid, other most pressure flow of water through the reduced pressure hole board, reduced pressure orifice plate forms a low pressure area. Squeeze out of the bubble fluid displacement by foam liquid pipe pressure relief hole in the area of low pressure after the board place, because of the dual role pressure suction and into the main channel of foam proportion mixer, and water pressure mixture of 3% or 6% of the proportion of the bubble mixture, foam fire extinguishing system for use. Tank pressure type foam mixing ratio device is mixed high precision than use the traffic pressure range pressure losses small, etc.

(2) Pump into the balance pressure type hybrid method

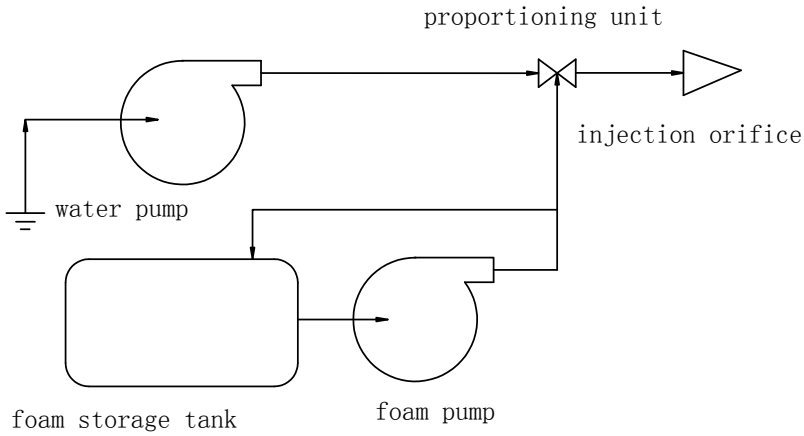

Fig. 5 Pump pressure balanced mixing method

When working, foam pump pumps a part of liquid into a bubble of mixer, while another shares through balance pressure flow control valves back into the liquid tank foam. Balanced pressure control valves that installed in reflux pipe consist of valve diaphragm ,chamber and throttle valve, the diaphragm chamber bottom is linked together through the catheter to the bubble pump export pipeline, the upper are interlinked through the catheter to the water pipe, when water pressure rises, the system of water increases, the bubble liquid supply should also increase, this time the diaphragm drive stem downward, reducing liquid foam mouth throttling back to flow, supply system of foam fluid flow is increased, and vice versa.

Pump into the balance pressure type foam proportion mixing device used by the foam liquid tank is atmospheric pressure tank, it is safe to use, reliable, and mixing ratio high precision, low pressure drop, it is suitable for flow pressure range, foam liquid reserves bigger, and many other advantages.

5. Summary

This paper first analyses existing foam proportion mixer and make out that tank pressure type and pump into the balance pressure type foam ratio are applicable on the sea. In reality, the use of foam mixer on the sea is backward; therefore, this paper proposes a new type of sea foam used in fire system of mixing ratio device. Above two kinds of new hybrid device theoretically possible, and in developed countries has been in practice and development. Finally, the government and the society should in this field as soon as possible invest and research, research and develop to promote the use, which produce the huge social benefits and economic benefits.

Acknowledgement

This work was supported by National Natural Science Foundation of China (No. 51075258), Shanghai Natural Science Foundation (No. 09ZR1421800). Their supports are gratefully acknowledged.

References

[1] L. Zheng. Petrochemical Dock Port on the Characteristics and Fire Prevention Measures, *Water fire*, Vol. 5, pp. 28-31, 2009.

[2] Z. J Xue and C. J Xu. Fixed Deck Foam Fire System Security Check, *Ship and Ocean Engineering*, Vol.1, pp. 136-138,2009.

[3] X. F Zhou. Oil Tanker Goods Oil Tank Fire Area Structure, Fire-Fighting Facilities Examination,*Water fire*, Vol. 1, pp. 32-35, 2006.

[4] China classification society. *Ships fire guidelines*, people's traffic press, 1999.

[5] Z.J Yang. *Pump Into the Balance Pressure Type Foam Mixing Ratio Device Design*, Shanghai Jiaotong University, 2003.

[6] Y. X Mi. Several Bubble of Mixing Ratio of the Device Short and Long, *Fire control technology and product information*, Vol. 12, pp. 11-14, 2000.

[7] Z. J Yang. Pump Into the Balance Pressure Type Foam Mixing Ratio Device Design, *Fire science and technology*, Vol. 22 , No. 3, pp. 181-182, 187, 2003.

[8] J. Cheng. Showing Ship for Fire Extinguishing System Structure and Check, *Water fire*, Vol. 3, pp. 31-32, 2011.

[9] L. Wang and J. Y Pu. The Naval Ships Fire Proofing Performance-Based Design, *Ship and Ocean Engineering*, Vol. 1, pp. 104-107, 2007.

[10] Z. J Wang. Stationary Deck Foam Extinguishing System Security Check Discussion. *China Water Transport*, Vol. 11, pp. 24-25, 2007.